UNIVERSITY OF SOUTHAMPTON

Faculty of Natural and Environmental Sciences
Chemistry

Relaxation of Longitudinal and Singlet Nuclear Spin Order as a Function of Solvent Viscosity

by

Aliki Moysiadi

Thesis for the degree of Master of Philosophy

June 2018

UNIVERSITY OF SOUTHAMPTON

Abstract

Faculty of Natural and Environmental Sciences
Chemistry

Master of Philosophy

Relaxation of Longitudinal and Singlet Nuclear Spin Order as a Function of Solvent Viscosity

by
Aliki Moysiadi

Extending the storage time of nuclear spin order is an important issue in modern NMR spectroscopy since many NMR and MRI applications are limited by the lifetime of spin states. Under normal circumstances the survival of spin magnetization is limited by longitudinal relaxation (T_1) which brings the magnetization back to equilibrium within a few seconds. The conversion of longitudinal into singlet order can extend that lifetime to tens of minutes up to an hour.

Most nuclear spin relaxation mechanisms in liquids are a function of the correlation time τ_c of the molecule, which is linked to the molecular tumbling, and inversely proportional to viscosity. Therefore a lower viscosity would reduce the influence of those mechanisms. The increase in the lifetime of longitudinal (T_1) and singlet order (T_S) is shown here as the viscosity of common organic solvents decreases.

The study includes measurements in liquid and supercritical CO_2, that offer an extremely low viscosity regime. The further extension of spin order lifetimes for a singlet bearing molecule in liquid CO_2 is presented. There appears to be an upper limit to the extension of the singlet order lifetime that is caused by relaxation mechanisms acting in different directions.

Contents

List of Tables

List of Figures

Acknowledgements

I would like to take this opportunity to thank my supervisor Dr. Giuseppe Pileio for the guidance and support he provided throughout the period of my candidature, as well as my co-supervisor Prof. Malcolm H. Levitt for his expert advice and encouragement.

I would like to also thank Dr. Francesco Giustiniano and Dr. Lynda J. Brown without whom this work would have not been possible. Dr. Giustiniano for designing and creating crucial elements of the equipment used for experiments and Dr. Brown for providing chemicals.

I would like to thank all of my colleagues in the Magnetic Resonance section for creating a pleasant working environment. It has been great collaborating with you and I will miss you all deeply. I am particularly indebted to James Eills and Christian Bengs for their patience as well as fruitful discussions on NMR and life. I really appreciate the time you invested. I am also really grateful to Dr. Karel Kouril, Dr. Benno Meier, Dr Hana Kourilova, Dr. Stuart Elliott and William Hale for their support and friendship.

I would also like to thank my family and friends for supporting my decisions and being there for me even from a distance. I would like to thank especially my closest friends, Matina and Athina for their views in life and their input in mine. Last but not least, I would like to thank my partner, Dr. Neil J. Wells for his unlimited patience and understanding throughout writing this thesis and my life in general.

1 Motivation of the Project

The limited lifetime of the signal generated in NMR spectroscopy represents one of its major limitations. Great efforts are being made in order to extend the lifetime of the magnetization. Elimination of the most prevalent relaxation mechanism results in extended lifetimes. Such an extension is achieved by accessing long lived states, such as singlet states and storing the magnetization in that form. This study is concerned with the manipulation of the viscosity of the medium in order to preserve magnetization and singlet order even further.

The longitudinal relaxation time constant, T_1, is primarily a property of the molecule. Molecular motion causes fluctuations in the nuclear spin interactions and therefore induces relaxation [2]. The relaxation rate in liquids is proportional to the correlation time, τ_c, of the molecule, which is in turn proportional to viscosity. Therefore, solvents of lower viscosity are expected to preserve the magnetization for longer. In this study we verify this relationship and present results concerning the relationship between the lifetime of the singlet order (T_S) and the solvent viscosity.

The investigation involves examining the behaviour of two singlet bearing molecules in deuterated organic solvents across a range of varying viscosity values in three different magnetic fields. In order to extend the study further, supercritical fluids were employed. Supercritical fluids exhibit viscosities intermediate to those of gases and liquids, occupying a region that is an order of magnitude less viscous than liquids.

CO_2 in particular has a viscosity of 0.06 mPa*s around the critical point, depending on the exact pressure and temperature [3]. To put that into context, the literature value for methanol at 25°C is 0.55 mPa*s. [1] There is then scope for extending the lifetime of spin order by as much as an order of magnitude.

The low sensitivity NMR suffers from as a technique, poses a limitation to its applications whether those take the form of spectroscopy or imaging. A magnetic field of 21 T, corresponds to a resonant frequency of 900 MHz for protons. Even then, despite being the most sensitive of the nuclei, the ^1H, are only polarized to 70 parts per million. [4]. Hyperpolarization is an all encompassing term used to denote enhancement of the standard polarization of the nuclear spins. Different techniques employed involve Optical Pumping, Parahydrogen Induced Polarization (PHIP) and Dynamic Nuclear Polarization (DNP).

It is hoped that the findings of this study could be used in conjunction with hyperpolarization, resulting in both enhanced and long lived NMR signals. In fact, supercritical CO_2 has been used as a solvent for Overhauser DNP at high magnetic fields. It was discovered that the maximum polarization enhancement achieved for ^1H benefits from low viscosity.[5]

2 Brief Introduction on NMR

Nuclear Magnetic Resonance (NMR) Spectroscopy is a powerful technique. Its many applications include structure elucidation of chemical compounds, studies of the conformation of proteins in space, ligand binding, diffusion and transport studies and of course magnetic resonance imaging (MRI).

2.1 Nuclear Spin

NMR spectroscopy has its basis in the magnetic properties of nuclei. Those arise through spin. Spin is an intrinsic property of a particle, much like mass and charge. It is a form of angular momentum which is however not caused by rotation, but exists on an intrinsic, quantum mechanical level. For that reason, spin is quantized. A spin quantum number S can only assume values of 1/2, 1, 3/2, and so on. Particles with spin S have 2S+1 degenerate sublevels. Under the presence of an external field (magnetic or electric), this degeneracy is lifted.

Nuclei consist of particles, protons and neutrons. Many nuclei of interest possess spin. The measure of the spin of nuclei is called the nuclear spin quantum number, I, and can assume positive values that are integer or half integer. For the purposes of this report, nuclei with $I = 1/2$, will be exclusively considered. Commonly encountered examples among those include: ^{1}H, ^{13}C, ^{15}N and ^{31}P [6].

A nuclear state with spin I is degenerate and has $2I+1$ sublevels. Application of an external magnetic field leads to an interaction between the spins and the magnetic field. In the presence of a magnetic field the degeneracy will be lifted and a spin-1/2 nucleus will have $2 \times 1/2 + 1 = 2$ energy sublevels. This is called the Zeeman effect. Transitions between those energy levels in a magnetic environment are studied with NMR.

Under the influence of a magnetic field, the nuclei undergo a type of motion called precession [7]. The Larmor frequency (ω^0) gives the angular velocity of the nuclear precession and is proportional to the magnetic field:

$$\omega^0 = -\gamma B^0, \tag{1}$$

where B^0 is the magnetic field and γ is a proportionality constant characteristic for each nucleus, called the gyromagnetic ratio.

The sign of the Larmor frequency indicates the sense of the precession. A negative Larmor frequency, which corresponds to a positive value of gyromagnetic ratio, as in the case of protons, corresponds to clockwise precession. If the gyromagnetic ratio is negative, then the sense of precession is anti-clockwise.

2.2 Magnetism

Particles have a magnetic moment in the same way they possess spin. In fact, the two properties are linked and proportional to each other through the relationship:

$$\mu = \gamma I, \tag{2}$$

In the absence of a magnetic field, the magnetic moments in a sample are distributed isotropically. This means that they can point in every possible direction.

Within a field the spins experience precession. The reason why they do not simply align themselves with the implemented field is the simultaneous existence of the angular momentum.

2.3 Magnetization

Since the precession does not align the spins with the field, it does not create a net magnetization that can be observed macroscopically. The presence of other, local magnetic fields within a sample, generated by electrons or other nuclei, add up into a different, time-dependent microscopic field for each spin, depending on its environment.

Those fluctuating microscopic fields interfere with the angle of precession and change it ever so slightly. Since this imperceptible change in the precession angle occurs, the motion of spins is no longer isotropic. As such it can be biased towards the orientation that proves to have the lowest energy. The anisotropic distribution which is eventually formed, is towards the direction of the magnetic field and involves a net magnetization at a state of thermal equilibrium [6].

The system can be perturbed from equilibrium and in order to extract information from the system, most NMR experiments start by doing so. The most common way for that to happen is by application of radiofrequency (rf) pulses or field cycling. After perturbation and since the system is left under the influence of the static magnetic field alone, the nuclei tend to return to their original state of equilibrium.

As the perturbed system starts to precess under the influence the magnetic field, the precession motion induces a current in the detector coils producing an oscillating signal. This oscillating signal is what is detected in the detector coil of the spectrometer.

The detected signal is called the free induction decay (FID). In an ideal situation, the signal would not decay, but rather be preserved, oscillating forever. However, reality is different. As mentioned, the spins do not only experience the external magnetic field, but also the magnetic fields generated by electrons or other nuclei. In general the overall field experienced by an individual spin varies with time. That results into the precession not persisting infinitely. Eventually the spins return to their thermal equilibrium, because of the effect of the fluctuating microscopic fields, as described above. This process is called Relaxation.

2.4 Relaxation

By the term relaxation we refer to the process which restores the spin system to its equilibrium through the interaction with the thermal molecular environment [6]. The types of relaxation processes that are encountered can be categorized into either longitudinal relaxation or transverse relaxation.

Longitudinal relaxation

Longitudinal relaxation, also known as spin-lattice relaxation, is the process by which the magnetization is restored parallel to the main magnetic field (commonly defined along the z-axis). To characterize this process, a time constant is used, called "Longitudinal relaxation time constant" or T_1. It is effectively giving the measure of the relaxation rate of the z-component of the magnetization following excitation [8].

$$M_z = M_0(1 - e^{-t/T_1}), \tag{3}$$

Sometimes it is useful to think in terms the recovery rate of the magnetization which is:

$$1/T_1 = R_1, \tag{4}$$

R_1 is called "longitudinal relaxation rate constant". However, more often than not, the word "constant" is dropped for both T_1 and R_1 and the two quantities are referred to as "time" and "rate" respectively.

Transverse relaxation

The concept of transverse relaxation is introduced to describe the loss of coherence in the motion of individual spins [9]. Transverse relaxation is also known as spin-spin relaxation. In order to characterize this process, another time constant is introduced, T_2.

Correlation Time, τ_c

The term stochastic is used to describe random probability distribution or a pattern that cannot be predicted precisely but may be analyzed. Stochastic processes are important in NMR relaxation theory [9] because of the random motion of molecules.

Correlation time is the measure of the persistence of correlation between values of stochastic processes at different points in time. The correlation time effectively is a measure of the memory the system retains of where it has previously been.

The autocorrelation function $G(\tau)$, correlates a stochastic process Y(t) with itself in different points in time:

$$G(\tau) = G(t_2 - t_1) =< Y(t_1)Y(t_2) >=< Y(t)Y^*(t+\tau) > \tag{5}$$

The final equality is true only when the function Y(t) is complex as is often the case.

$$G(\tau) = G(0)e^{-|\tau|/\tau_c} \tag{6}$$

It can be shown [9] that:

$$\frac{1}{T_1} = R_1 = 2G(0)\frac{2\tau_c}{1 + \omega_0^2\tau_c^2} \tag{7}$$

When the molecular motion is rapid then $\omega_0^2\tau_c^2 \ll 1$. That condition reflects the "extreme narrowing region" which is the region where the relaxation rate is not dependent on the magnetic field.

This results in:

$$\frac{1}{T_1} = R_1 \propto \tau_c \tag{8}$$

It can be proven that in the case of a relaxation mechanism like the dipole-dipole relaxation [9]:

$$\tau_c = \frac{V\eta}{k_B T} \tag{9}$$

Where:

- η is the solution viscosity
- V is the volume of the molecule
- T is the temperature and
- k_B is the Boltzmann Constant, $k_B = 1.38066 \cdot 10^{-23}$

Therefore:

$$\frac{1}{T_1} = R_1 \propto \tau_c \propto \eta \tag{10}$$

2.4.1 Relaxation Mechanisms

Relaxation is a composite phenomenon and there are various mechanisms contributing to it. In the particular case of a two spin-1/2 system in solution state NMR, the relevant relaxation mechanisms that need to be taken into account are typically the dipolar (DD), the chemical shielding anisotropy (CSA) and spin-rotation (SR).

The relationship which describes this is presented in the form of Equation 12:

$$\frac{1}{T_1} = \frac{1}{T_{1,DD}} + \frac{1}{T_{1,CSA}} + \frac{1}{T_{1,SR}} + ... \tag{11}$$

Dipolar Relaxation

The Dipolar Relaxation mechanism is generated through the direct (through space) dipole-dipole coupling between spins. Through molecular tumbling, the direction and magnitude of the local magnetic field the spins impose onto one another change, causing relaxation. It is the non-secular part of the coupling which gives rise to relaxation in isotropic liquids, while the secular part is averaged.

DD is the most dominant relaxation mechanism when it comes to spin-1/2 nuclei. The extended lifetime of singlet states is due to the fact that they are immune to the part of the DD interactions that describes the coupling between the two members of the spin-pair. Couplings to other spins, which in general exist, act as mechanisms of singlet relaxation. [10]

$$\frac{1}{T_{1,DD}} \propto \tau_c \tag{12}$$

Chemical Shift Anisotropy Relaxation

The external magnetic field induces electron currents around the molecules. Those electron currents generate local fields that vary in magnitude and direction depending on the orientation of the molecule with respect to the external magnetic field. The molecular motion causes fluctuations in the field each spin is experiencing due to its neighbours and that leads to relaxation.

The main characteristic of the CSA mechanism is that T_1 is inversely proportional to the square of the magnetic field. This means that CSA becomes a relevant relaxation mechanism in higher magnetic fields. In general, assuming the extreme narrowing regime and that the tumbling of the molecule of interest resembles that of a rigid spherical object, Equation 14 holds true:

$$\frac{1}{T_{1,CSA}} \propto \tau_c \tag{13}$$

Spin-Rotation Relaxation

This mechanism is prevalent in the relaxation of spins in small symmetric molecules. It originates from the magnetic field produced by rotating electronic charges. In this particular case of relaxation it can be shown that [9]:

$$T_{1,SR} \propto \tau_c \tag{14}$$

2.5 Singlet States

On numerous occasions, the so called "long lived spin states" have been observed [11, 12], formed by clusters of coupled nuclear spins. When it comes to a long lived state comprised of more than two nuclei, its existence is strongly dependent on the geometry of the nuclei, the relative magnitudes of spin-spin couplings and their chemical shift differences [13].

When the system under examination only includes two-1/2 spins of the same nucleus, the long lived state is called a singlet. Singlet states can have a decay constant, now called T_S which is at least one order of magnitude bigger than the corresponding T_1 [14].

Singlet states are of primary importance in this project. A singlet state is formed between two-1/2 nuclei as a result of their combined states, along with a group of states called triplet states:

$$|I_1 - I_2| = 0 \Rightarrow I_3 = 0 \rightarrow M_I = 0 \tag{15}$$

$$|I_1 + I_2| = 0 \Rightarrow I_3 = 1 \rightarrow M_I = \{-1, 0 + 1\} \tag{16}$$

Where M_I is the azimuthal quantum number. The term "triplet state" is used to underline the three-fold degeneracy of a state with $I = 1$. A characteristic property of the singlet state is that the two spins are combined in such a way as the total spin I is zero, thus making a non-magnetic state out of two magnetic ones.

The Dirac notation for the singlet and triplet is given in Equations 18-21 [10]:

$$|S_0\rangle = \frac{1}{\sqrt{2}}(|\alpha\beta\rangle - |\beta\alpha\rangle) \tag{17}$$

$$|T_{+1}\rangle = |\alpha\alpha\rangle \tag{18}$$

$$|T_0\rangle = \frac{1}{\sqrt{2}}(|\alpha\beta\rangle + |\beta\alpha\rangle) \tag{19}$$

$$|T_{-1}\rangle = |\beta\beta\rangle \tag{20}$$

A particularly interesting property of the singlet state is its immunity to dipolar relaxation, which for a spin-1/2 pair system is the most prominent source of signal decay [11, 15].

Singlet states are anti-symmetric to spin exchange while triplet states are symmetrical. For the former, the sign changes with the exchange of the two spins while for the latter it remains unaltered. Immunity is caused by the fact that the dipolar interaction is also symmetrical. Therefore, it does not mix with the singlet state [15].

The population imbalance between a singlet state and the triplet states is called singlet order.

Chemical Equivalence

In systems that exhibit chemical equivalence, the nuclei of the spin pair have the same chemical shift. In that regime all states are exact eigenstates of the nuclear spin Hamiltonian, and that makes accessing the singlet state rather difficult. Symmetry makes the singlet a possibility, but also prevents it from being observable. A simple population

transfer does not suffice as manipulations in the form of pulses will have a symmetric impact since the two spins are indistinguishable [2].

Chemical Inequivalence

In the case that the symmetry between the spin pair is broken, they possess different chemical shifts thus becoming inequivalent. Manipulation of the chemical shift difference of an inequivalent homonuclear spin pair allows singlet handling at high field [12]. Therefore, in that regime, accessing the singlet state becomes slightly easier. However, that very same pre-requisite to a singlet's observation is also introducing a path to its relaxation and at the same time, maintaining the singlet order by suppressing the chemical shift difference becomes non trivial [16].

Suppression of the chemical shift difference can be achieved in a variety of ways such as [2, 16]:

1. **Field-cycling**, involving changes in the magnetic field the sample experiences by physically transporting it to lower magnetic field values (e.g. outside of the spectrometer) exploiting the fact that singlet and triplet states both become exact eigenstates of the Hamiltonian at zero magnetic field [15, 17].

2. Resonant radiofrequency field application. In principle, this technique suppresses the singlet to triplet interconversion, effectively "locking" the singlet state in high magnetic field and is therefore colloquially known as **Spin Locking**.

Spin locking is not an ideal solution in the case of a spin pair with large chemical shift difference because it would cause heating of the sample and possible hardware damage.

Near Equivalence

A "near-equivalence" or "extremely-strong-coupling" regime of spins is the state which describes a spin-1/2 pair of nuclei which has a chemical shift difference smaller than the spin-spin coupling between them. Such a system can be designed by starting from an equivalent molecule whose symmetry is lifted by introducing a slightly different substituent far enough from the site. In such cases, it has been shown that singlet order can be generated directly in high magnetic field, and most impressively, without spin locking being essential (although the latter remains beneficial when implemented) [14]. The "near-equivalence" regime is the one of interest for this experiments and we shall not consider the others further.

2.6 Supercritical CO_2

Supercritical fluids are substances at pressures and temperatures above their critical values. The term critical temperature refers to the value of temperature that once exceeded, the substance can no longer be a liquid. Respectively, critical pressure is the value above which the substance cannot be a gas. This results in a fourth phase, which is called supercritical. [18]

The supercritical regime gives access to a variety of different possibilities, as the properties of the supercritical substance become intermediate between those of liquid and gas. Supercritical fluids typically have a density similar to that of liquids, in a region between 0.1-0.8 g/cm^{-3}. In the case of supercritical CO_2, the value of density corresponds to 0.47 g/cm^{-3} for the pure substance. Contrarily, supercritical fluids demonstrate diffusion coefficients and viscosity values closer to those of gases. [19] CO_2 in particular has a viscosity of 0.06 mPa*s around the critical point, depending on the exact pressure and temperature [3]

2.6.1 Supercritical CO_2 as a Solvent

The use of supercritical fluids as solvents is not something novel. In fact, the use of supercritical fluids as a mobile phase for chromatography separations, which is the most popular use, was first suggested more than fifty years ago. [20] Supercritical chromatography has a multitude of applications, ranging from industrial to pharmaceutical to preparatory to extraction. The use of supercritical CO_2 is particularly advantageous in food processing. [18]

There is a multitude of reasons why CO_2 is particularly popular as a supercritical solvent. As a gas, CO_2 is inert, non-flammable and relatively inexpensive. [21] It is also non-explosive and non-toxic. These properties make it easy to handle and safe to liquefy, solidify and store. [19] [22]

CO_2 has relatively moderate critical conditions with a critical temperature at 31 ^{o}C and a critical pressure at 74 bar. [23] This results in a low critical point, which is an attractive feature. [24] It is also miscible with a variety of organic solvents, which gives access to a whole new polarity range if that is desirable.

CO_2 is a natural component of the atmosphere. However, fossil fuel burning and other human-induced activities have resulted in an increased input. [25] Commercially used CO_2 is reclaimed from industrial processes such as ethanol, coke, ammonia, and natural gas production, as well as the burning of fossil fuels for the generation of electricity. [22] CO_2 as a solvent has the additional advantage of being easy to remove, by reduction of pressure and venting. [26] Since commercial CO_2 is already an industrial byproduct, the net environmental impact is zero and is considered a "green" solvent. [27]

Supercritical CO_2 is not new to NMR. Supercritical fluid chromatography has been coupled with nuclear magnetic resonance, allowing acquisition of ^{1}H spectra as far back as 1997, also reporting the extension of longitudinal lifetime T_1. [28] Supercritical CO_2 has also been successfully used as a solvent for Overhauser DNP at high magnetic fields, resulting in increased polarization enhancement which is attributed to the low viscosity.[5]

3 Methods

3.1 Experimental Conditions

All experiments conducted were performed on either a 300 MHz Bruker Avance III spectrometer, a 500 MHz Bruker Avance III spectrometer or a 700 MHz Bruker Avance Neo spectrometer. The details are presented in Table 1. The data produced on Topspin were fitted with Wolfram Mathematica to derive the fitting errors.

Spectrometer	300 MHz	500 MHz	700 MHz
Magnetic Field	7.05 T	11.7 T	16.4 T
Magnet	Oxford Widebore	Bruker ActiveShield II WB	Bruker Ascend 700 NB
Console	Bruker Avance III	Bruker Avance III	Bruker AVANCE NEO
Probe	10mm imaging	5MM TBO	5mm TCI prodigy
Software	Topspin 2.0	Topspin 3.2	TopSpin 4.0.2b14

Table 1: Details of the spectrometers used, listing the magnetic field, the type of magnet, the console, the probe and the software used while conducting experiments.

3.2 Main Experiments Performed

3.2.1 Saturation Recovery

For the measurements of the longitudinal relaxation time T_1 the method used was saturation recovery and the pulse sequence can be seen below in Figure 1. This experiment works on the principle of saturating the signal by pulsing rapidly. Denoted τ is the delay between pulses and n is the number of loops of delays and pulses. A variable delay time T is allowed for the magnetization to build up along the field and then finally a 90x pulse converts the longitudinal into transverse magnetization and the FID is recorded.

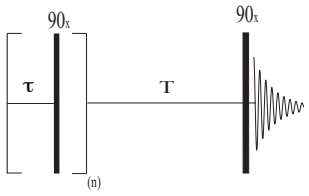

Figure 1: A typical Saturation Recovery pulse sequence

3.2.2 Magnetization to Singlet - M2S

In this work we are concerned with high field measurements at the "near-equivalence regime". A pulse sequence suitable for converting longitudinal magnetization into singlet order has been previously developed, called M2S, which serves as shorthand for Magnetization-to-Singlet. [14] [29] This sequence was used for all T_S measurements mentioned in this project and is described in Figure 2.

The first pulse of the sequence (90_y) has the effect of converting longitudinal magnetization into single quantum coherences between the central triplet and each of the outer triplets.

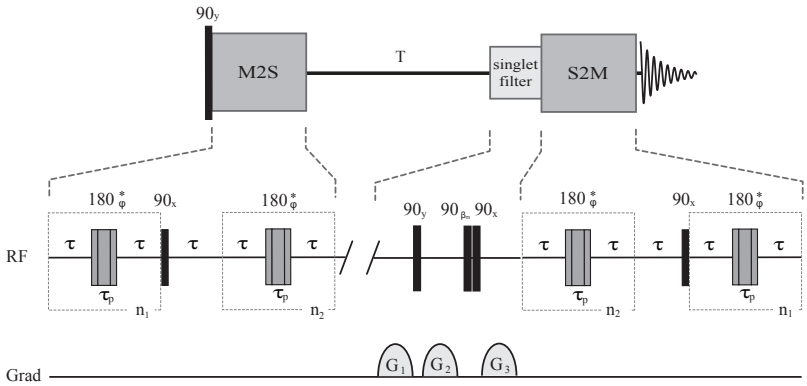

Figure 2: Magnetization to Singlet and back to Magnetization pulse sequence. τ is a time delay equal to 1/4J, τ_p is the duration of the composite pulse, n_1 and n_2 are the number of loops of the J-synchronised spin echoes. G_1, G_2 and G_3 are the gradients used in the singlet filter.

The M2S block has four components as can be seen in the expansion of it in Figure 2. Those have the following effects:

1. The single quantum coherences between the central triplet and the outer triplets are transformed into coherences between the singlet and each of the outer triplet states by a π rotation into the S_0 - T_0 subspace. This is achieved by implementing a J-synchronised Spin Echo. This consists of a delay τ which is 1/4J, where J is the J-coupling, a composite π-pulse and another delay τ, looped n_1 times.

2. The coherences between the singlet and each of the outer triplet states are transformed into zero quantum coherences between the singlet state and the central triplet state by a 90_x pulse.

3. The energy difference between the central triplet, T_0, and the singlet, S_0, is J. A delay τ (equal to 1/4J) induces a phase rotation of the S_0 - T_0 coherence by $\pi/2$. This delay has the purpose of changing the sign between the coherences. If this delay is missing then the following JSE sequence has no effect. The reason for this is that a difference between the states is needed.

4. The coherences between the central triplet and the singlet state are converted into populations. This is achieved with a second J-synchronised Spin Echo sequence. This is identical to the first apart from the fact that it has exactly half the number of loops (n_2) as the desired rotation in the S_0 - T_0 subspace is by $\pi/2$ instead of π in this case.

A variable delay T is used, followed by a singlet filter that makes use of gradients in order to exclude any magnetization that has not been converted into singlet from the final step. The final step of the pulse sequence is denoted S2M, shorthand for "singlet to magnetization" and it the exact inverse of the M2S block.

The following equations define the parameters:

$$\tau = \frac{1}{4J}$$

where J is the J-coupling between the two spins of the spin pair and

$$n_1 = \frac{\pi}{2\theta}$$

where θ is defined by

$$tan(\theta) = \frac{2\pi J}{\omega_\Delta}$$

and ω_Δ is the chemical shift difference between the two nuclei consisting the spin pair. The value of n_1 is always rounded to the closest integer. n_2 is simply half of n_1.

3.2.3 Diffusion Ordered Spectroscopy - DOSY

Diffusion measurements were performed to determine the viscosity (η) values experimentally. All diffusion experiments took place at 16.4 T, according to Table 1. The pulse sequence implemented was originally developed by A. Jerschow [30],[31]. It is now a standard Bruker sequence that can be found under the name dstebpgp3s. The pulse sequence can be seen in Figure 3.

It is a 2D sequence for diffusion measurement that uses a double stimulated echo, bipolar gradient pulses and three spoil gradients. Its advantage over simpler pulse sequences is that compensates for convection.

Throughout our experiments there were strong indications of convection interference, and that was the primary reason this pulse sequence was selected. A secondary reason was that the diffusion experiments conducted were run using a cryoprobe which is known to generate convection as well.

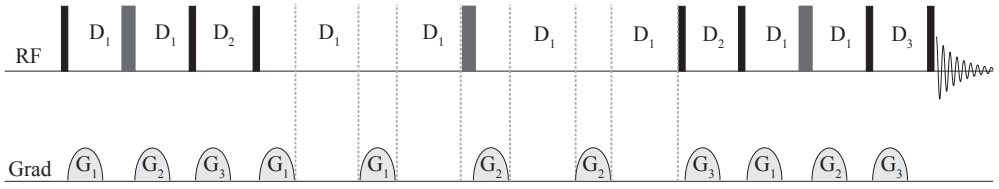

Figure 3: Double stimulated echo with bipolar gradient pulses and three spoil gradients. The 90° pulses are shown as black rectangles and 180° pulses are shown as gray rectangles. For every pulse, phase cycling is used. The delays are denoted with D and the gradients with G. D_1 is the delay used for gradient recovery and is a set number. D_2 and D_3 are delays calculated from the experimental parameters.

The 90° pulses are shown as black rectangles and 180° pulses are shown as gray rectangles according to standard notation. For every pulse, phase cycling is used.

- G_1 is a gradient pulse defined as δ*0.5.
- G_2 is a gradient opposite to G_1.
- G_3 is a spoil gradient with a set value (600 μs).

where δ is the gradient strength.

D_1 is the delay used for gradient recovery and is a set number (0.2 ms). D_2 and D_3 are delays calculated from experimental parameters. D_2 depends on Δ (the diffusion time), δ, D_1, G_3 and the values for the 90° and 180° pulse. D_2 depends on a parameter called eddy current delay which is set to 5 ms and G_3.

4 Experimental

4.1 Compound selection

Not every compound can support long lived states. In order to have the potential of accessing the singlet state and also exhibit reduced relaxation rate, a candidate molecule needs to conform to certain criteria. Those can be summarized in the following points [8], [32]:

1. In order to have the capacity to create and access the singlet state in the "near-equivalence" regime in which our interest is focused:

   - The molecule of interest must have a pair of spin-1/2 nuclei.
   - The nuclei consisting the spin pair must be magnetically inequivalent.
   - The chemical shift difference between the two nuclei of the spin pair needs to be significantly smaller than the J-coupling between them

   The latter two requirements are usually met by having a symmetric environment around the spin pair, with the symmetry broken away from the spin pair.

2. In order to reduce the effect of dipolar and scalar coupling relaxation

   - The spin pair needs to be as far away as possible from other spin active nuclei (e.g. ^{1}H).
   - While ^{2}H is a better option than ^{1}H, it is also required to be as far away as feasible from the spin pair.
   - The molecular environment close to the spin pair needs to be conformationally rigid in order to restrict motion that would result to relaxation.
   - The spin pair should be shielded against paramagnetic agents, such as metal ions and molecular oxygen.

4.2 Substituted Naphthalenes

The molecule selected for the main experiments conducted was a naphthalene derivative. The synthetic process which leads to it is reported elsewhere [32]. The generic structure of the compound can be seen in Figure 4. The primary reason for selecting this molecule is that it has the longest singlet lifetime known so far on a purpose-made compound [8]. Moreover, it has been studied extensively in previous investigations and is well known to this group and our collaborators.

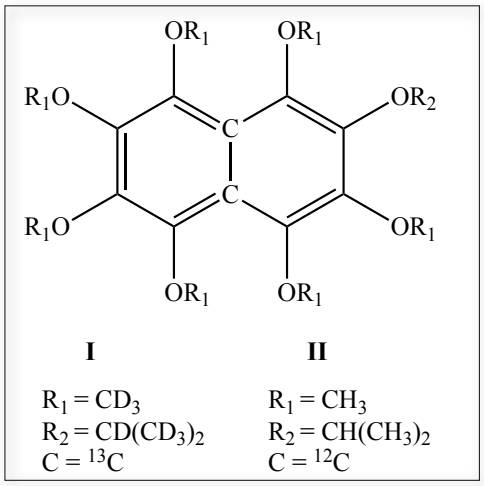

Figure 4: Generic structure of the Naphthalene derivative. Compound **I** is the fully deuterated, ^{13}C labelled version of the compound, the one that can access the singlet state, while **II** is the protonated, unlabelled version of the compound which was used for solubility trials and preliminary investigations.

Two versions of the compound were used:

- The fully deuterated, ^{13}C labelled version of the molecule; $1,2,3,4,5,6,8-heptakis-(methoxy-d_3)-7-((propan-2-yl-d_7)-oxy)-naphthalene-4a,8a-^{13}C_2$, which for the purposes of this work will be referred to as **I**. Compound **I** has a molecular weight of 426.59 mg/mmol. Having been specifically designed to be able to access and retain the singlet state for a long time, it is the compound which currently holds the record for the longest T_S observed (>1h in room temperature solution in low field) [8].

- The protonated and unlabelled version; 2-isopropoxy-1,3,4,5,6,7,8-heptamethoxy-naphthalene which will be referred to as **II**. Compound **II** has a molecular weight of 369.44 mg/mmol. This molecule cannot access the singlet state and was used only for primary investigation as its synthesis is less expensive and relatively less laborious.

4.3 Substituted Acetylene

For a secondary set of experiments, an acetylene derivative, synthesized by Dr. Lynda J. Brown was selected. The molecular weight of compound **III** is 174.31 mg/mmol. The molecule is depicted in Figure 5. Its full name is $1-(ethoxy-d_5)-6-(methoxy-d_3)hex-3-yne-3,4-{}^{13}C_2-1,1,2,3,5,5,6,6-d_8$ but for the purposes of this work will be referred to as **III**. Compound **III** has a molecular weight of 174.31 mg/mmol.

The reason for selecting this particular compound was that it has been studied before [10],[33] and during previous investigations it had proved to be less prone to being affected by the Chemical Shift Anisotropy relaxation mechanism, which is proportional to the magnitude of the magnetic field.

Therefore, we expected it to have T_1 and T_S values independent of the magnetic field.

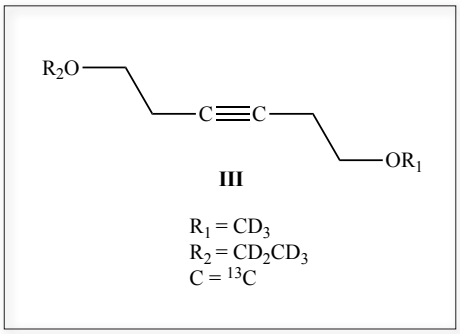

Figure 5: Structure of the Acetylene derivative. Compound **III** is the fully deuterated, ^{13}C labelled version of the compound and it was the only one that was used.

4.4 Sample Preparation

4.4.1 Solvent Selection

In order to study the effect viscosity has on the lifetime of the longitudinal and singlet order, six deuterated solvents were selected on the basis of their varying viscosity values. These were: acetone, chloroform, methanol, ethanol, dimethyl sulfoxide and t-butanol. Their viscosities for the protonated and deuterated isotopologues are reported in Table 2.

Solvent	**Viscosity**	
	Protonated Solvent (25°C)	Deuterated Solvent (20°C)
Acetone	0.31	0.34
Chloroform	0.54	0.57
Methanol	0.55	0.52
Ethanol	1.1	1.2
DMSO	2.0	2.4
t-Butanol	4.3	-

Table 2: Solvents selected for the experiments and corresponding viscosity in mPa*s. In the first column the viscosity for solvents at 25°C is given (Handbook of Chemistry and Physics (74th edition 1993-1994)) while the second column contains the viscosity of the deuterated equivalents at 20°C from http://www.science-and-fun.de/tools/solvents/

From this point forth when the viscosity of solvents is mentioned, we refer to the deuterated value. The sole exception is when it comes to t-butanol, for which the protonated value is used throughout this work, as there was no deuterated value found in the literature.

4.4.2 Substituted Labelled Naphthalene in Organic Solvents

A quantity of approximately 43 mg of **I** was dissolved in 0.5 mL of each of the solvents, thus forming a set of samples of 0.2 M. The exact values of weights and concentrations are summarised in Table 3.

Solvent	**Viscosity (mPa*s)**	**Quantity (mg)**	**Volume (mL)**	**Concentration (M)**
Acetone	0.34	44.2	0.5	0.2
Methanol	0.52	42.6	0.5	0.2
Chloroform	0.57	42.8	0.5	0.2
Ethanol	1.2	42.9	0.5	0.2
DMSO	2.4	42.9	0.5	0.2
t-Butanol	4.3	41.7	0.5	0.2

Table 3: Table listing the deuterated solvents used and their corresponding viscosity values along with the amount of **I** used in sample preparation, the solvent volume and the resulting concentration.

The samples were transferred into Wilmad low pressure/vacuum NMR tubes and each was degassed by bubbling Argon for a minimum time of 10 minutes. For the more

volatile solvents (chloroform and acetone), a reference tube filled with plain solvent was used to determine the correct volume while degassing.

4.4.3 Substituted Acetylene in Organic Solvents

A quantity of approximately 20 mg of **III** was dissolved in 0.5 mL of each of the solvents, thus forming a set of samples of 0.2 M. The exact values of weights and concentrations are summarised in Table 4.

Solvent	**Viscosity (mPa*s)**	**Quantity (mg)**	**Volume (mL)**	**Concentration (M)**
Acetone	0.34	19.5	0.5	0.2
Methanol	0.52	19.3	0.6	0.2
Chloroform	0.57	20.5	0.4	0.3
Ethanol	1.2	20.0	0.7	0.2
DMSO	2.4	20.0	0.5	0.2
t-Butanol	4.3	19.0	0.5	0.2

Table 4: Table listing the deuterated solvents used and their corresponding viscosity values along with the amount of **III** used in sample preparation, the solvent volume and the resulting concentration.

The samples were transferred into Wilmad low pressure/vacuum NMR tubes and each was degassed under nitrogen flow for a minimum time of 10 minutes. The reason for the variance in volumes is that the nitrogen flow was difficult to control resulting in different levels of evaporation. Since the final concentrations do not vary among themselves by much, we proceeded with the experiments.

5 Measurements of T_1 and T_S as a function of viscosity in common organic solvents

5.1 Motivation

The purpose of the experiments described below was to determine whether the longitudinal and singlet order lifetimes are inversely proportional to the viscosity of the solvent in which a substance is dissolved.

5.2 Measurements of T_1 and T_S as a function of viscosity in common organic solvents

5.2.1 Labelled Naphthalene

The results of the T_1 and T_S measurements on **I** for each of the different solvent environments (acetone, methanol, chloroform, ethanol, DMSO and t-butanol) at 7.05 T, 11.7 T and 16.4 T are presented in Table 5, in order of increasing viscosity. The data were collected once and the errors reported are fitting errors as calculated using Wolfram Mathematica.

Field (T)	**7.05**		**11.7**		**16.4**	
	T_1 (s)	T_S (s)	T_1 (s)	T_S (s)	T_1 (s)	T_S (s)
Acetone	26 ± 2	1959 ± 163	12.6 ± 0.4	485 ± 16	6.9 ± 0.2	149 ± 5
Methanol	16.9 ± 0.6	1278 ± 87	7.69 ± 0.06	249 ± 9	4.17 ± 0.03	92.0 ± 0.9
Chloroform	15.4 ± 0.6	819 ± 34	6.53 ± 0.06	217 ± 3	3.55 ± 0.02	73 ± 1
Ethanol	10.3 ± 0.4	673 ± 27	4.51 ± 0.05	174 ± 2	2.46 ± 0.02	59.0 ± 0.6
DMSO	4.5 ± 0.2	468 ± 41	2.37 ± 0.02	194 ± 8	1.26 ± 0.01	73 ± 1
t-Butanol	2.2 ± 0.1	141 ± 6	1.18 ± 0.05	35 ± 1	0.684 ± 0.003	13.7 ± 0.3

Table 5: T_1 and T_S measurements of **I** with corresponding fitting errors for each of the different solvent environments (acetone, methanol, chloroform, ethanol, DMSO and t-butanol) in order of increasing viscosity across three fields (7.05 T, 11.7 T and 16.4 T). The data were acquired once according to Table 1 and the samples were prepared according to Table 3.

The values of T_1 and T_S presented in Table 5 are plotted against the inverse of viscosity for all magnetic fields where experiments were conducted (7.05 T, 11.7 T and 16.4 T) in Figure 6. For all of the plots the viscosity values for the deuterated solvents have been used.

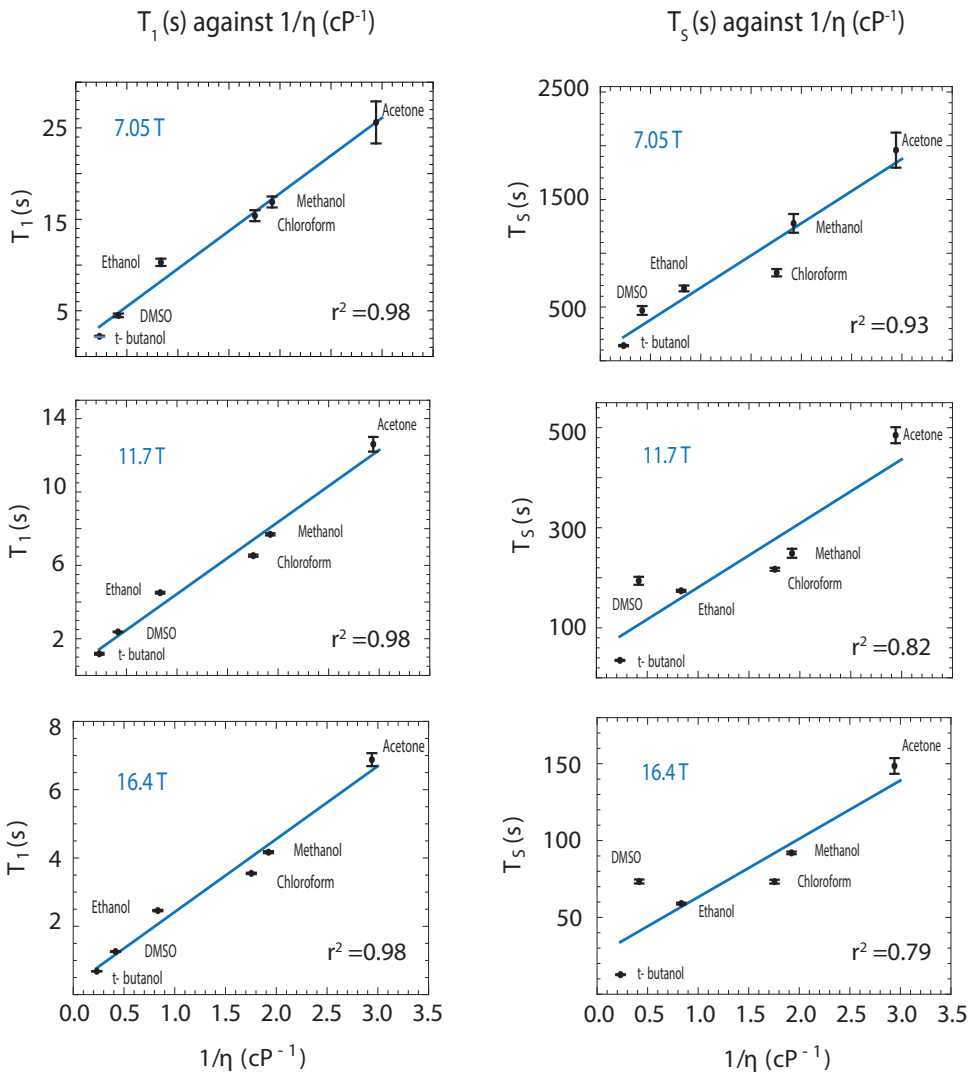

Figure 6: T_1 and T_S values of **I** plotted against the inverse of the viscosity $1/\eta$ of the dissolving medium for three magnetic fields (7.05 T, 11.7 T and 16.4 T).

Discussion

When T_1 and T_S values are plotted against the inverse of the viscosity as in Figure 6, correlation becomes apparent. There is a strong linear relationship between the longitudinal and singlet order lifetimes and the inverse of the viscosity as predicted by theory. This can also be verified by the r^2 values presented in Figure 6 and repeated in Table 6.

Field (T)	**r^2**	
	T_1 (s)	T_S (s)
7.05	0.98	0.93
11.7	0.98	0.82
16.4	0.98	0.79

Table 6: r^2 values which correspond to the quality of fit of T_1 and T_S measurements of **I** against the inverse of the viscosity of the dissolving medium across three different fields (7.05 T, 11.7 T and 16.4 T).

Overall, the T_1 values demonstrate good correlation with the inverse of the viscosity of the dissolving medium for each magnetic field. For the T_S, the data follow the same linear trend, although the quality of fit is not as good, particularly at high field. This could be attributed to the point of DMSO acting as an outlier. It can easily be observed in Figure 6 that the T_S values of **I** in DMSO appear to be higher than expected at higher fields. The reasons why this is happening are not clear.

When it comes to T_S values, the effect of the dipolar relaxation is by definition eliminated. Assuming that the remaining relevant mechanisms are CSA and SR, we are expecting CSA to be the most relevant mechanism, especially at high field, and especially for the more viscous solvents. Perhaps the deviation of DMSO from the line can be attributed to a reduced effect of CSA anisotropy on **I** in DMSO. Again, the reasons for this are unclear.

It is worth noting that at points **I** would precipitate out of solution as DMSO freezes around room temperature. The sample required heating prior to measurement. At 7.05 T the experiments were conducted at ambient temperature as the instrument does not have temperature control capabilities. The lab temperature is kept between 21-22 ^{o}C. At 11.7 T and 16.4 T the experiments were conducted at 22 ^{o}C.

In plotting the data there was no amendment made to the viscosity values found in literature. We assumed that in the regime of common solvent viscosity in which we were working, the viscosity values do not change significantly within a range of a couple of degrees ^{o}C or with the dissolution of compound in the solvent. For more accurate determination of viscosity values a viscosimeter is currently being built.

It is worth mentioning that the samples were stored for four months prior to their measurement at 11.7 T and twelve months prior to their measurements at 16.4 T and they were not re-degassed as to avoid changing their concentrations.

Conclusions

This series of experiments verified the prediction about a linear trend between the inverse of the viscosity $1/\eta$ and T_1 and proved that a similar trend holds for the T_S, for which no predictions had been made.

The positive results of those experiments were encouraging enough for us to extend the scope of this investigation to solvents with lower viscosity, such as supercritical fluids and in particular supercritical CO_2.

5.2.2 Substituted Labelled Naphthalene Sample Quality Control

The experiments discussed above, on the measurements of T_1 and T_S across three different fields (7.05 T, 11.7 T and 16.4 T) took place within the span of a year.

The samples were not prepared again, the ones described in Table 3 were stored and used throughout that period, without being degassed apart from that very first time. In order to ensure that they were in a good condition and had not been compromised in the meanwhile, the sample of **I** in t-butanol was selected as a reference point as the one with the shortest lifetime and therefore the easiest to measure.

As the original measurements took place at 7.05 T and consecutive measurements were conducted at higher fields, prior to each new measurement, the sample of **I** in t-butanol was measured again at 7.05 T.

The results are presented in Table 7, which shows the values of T_1 and T_S of **I** in t-butanol at the time of the preparation of the sample, four and twelve months later.

	I in t-butanol	T_1	T_S
1.	t_0	2.21 ± 0.06	141 ± 6
2.	t_0 + 4 months	2.19 ± 0.08	133 ± 5
3.	t_0 + 12 months	2.3 ± 0.1	129 ± 5

Table 7: T_1 and T_S measurements with corresponding errors for **I** in t-Butanol: 1. When the sample was fresh 2. After four months and 3. After twelve months.

Conclusion

There was no detrimental deviation in the values observed: in the case of molecular oxygen contamination, the results would vary greatly. For that reason we proceeded with the experiments using the original samples, without taking any further action.

5.2.3 Substituted Acetylene

Measurements on **III** in the common organic solvents under discussion were conducted only at 16.4 T. The results are presented in Table 8.

Solvent	**Viscosity (mPa*s)**	T_1 **(s)**	T_S **(s)**
Acetone	0.34	8.2 ± 0.1	249 ± 11
Methanol	0.52	6.40 ± 0.06	207 ± 11
Chloroform	0.57	4.50 ± 0.07	206 ± 4
Ethanol	1.2	4.43 ± 0.06	159 ± 7
DMSO	2.4	2.07 ± 0.02	-
t-Butanol	4.3	1.52 ± 0.02	23.7 ± 0.5

Table 8: T_1 and T_S of **III** with corresponding fitting errors for each of the different solvent environments (acetone, methanol, chloroform, ethanol, DMSO and t-butanol) in order of increasing viscosity at 16.4 T. Data acquired according to Table 1. The samples were prepared according to Table 4.

The values of T_1 and T_S measured are plotted against the inverse of viscosity at 16.4 T in Figure 7. For all of the plots the viscosity values for the deuterated solvents have been used.

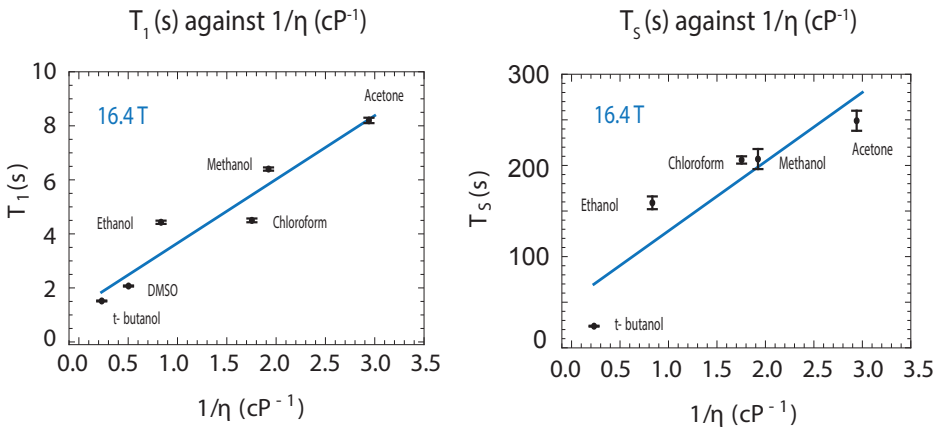

Figure 7: T_1 and T_S values of **III** plotted against the inverse of the viscosity $1/\eta$ of the dissolving medium for each of the different solvent environments (acetone, methanol, chloroform, ethanol, DMSO and t-butanol) at 16.4 T.

Discussion

The T_1 values of **III** exhibit good linear correlation against the inverse of the viscosity of the dissolving medium. While the relationship between the T_S values against $1/\eta$ is also linear, there are a few points that need to be brought into attention.

There is no T_S value of **III** in DMSO reported as it was impossible to determine the conditions for the transfer of magnetization to singlet in this case. The optimization that takes place prior to the main M2S sequence did not give meaningful results. This observation was also confirmed by simulation. As can be observed in Figure 8, the chemical

shift of ^{13}C in DMSO varies greatly compared to the rest of the solvents, which hints at a particularly strong interaction between the molecule and the solvent in that case.

As can be seen in Figure 7, the T_S value of **III** in t-butanol deviates greatly from the rest. At first it was assumed that the tube had not been sealed or degassed properly and was therefore contaminated with molecular oxygen and this was resulting in a reduced observed T_S value. However, even after degassing anew and measuring again, the results were identical.

It is interesting to note that the ^{13}C peak of **III** is not a singlet but it is split into a doublet (Figure 8). It is possible that in that particular solvent the molecule assumes such a conformation within the solvent that the chemical shift difference becomes greater than the J-coupling, thus giving rise to two signals instead of one.

This does not mean that the system does not meet the criteria for the transfer of magnetization to singlet order with the M2S pulse sequence. However, there is a strong solvent effect on the chemical shift, which varies greatly across the range of solvents used as can be observed in Figure 8.

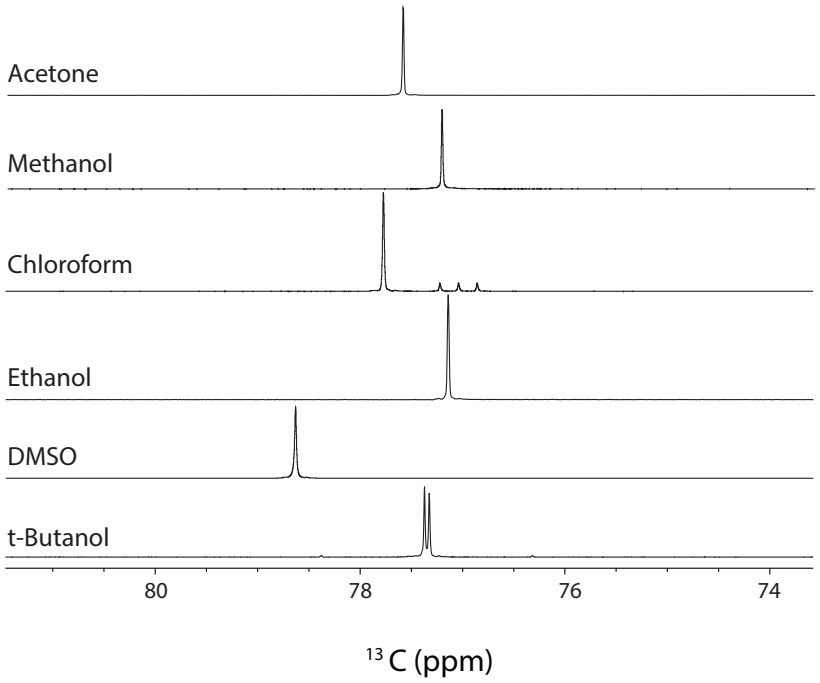

Figure 8: Multiple display of ^{13}C spectra of **III** in CO_2 for each of the deuterated solvents (acetone, methanol, chloroform, ethanol, DMSO and t-butanol). The triplet belonging to chloroform can also be seen in the chloroform ^{13}C spectrum. The samples was prepared according to Table 4.

Conclusions

This series of experiments on **III** provide additional evidence that the observed linear trend between T_1 and T_S values against inverse of the viscosity $1/\eta$ holds for a variety of systems. For that reason, we decided to extend the scope of the investigation to supercritical fluids and in particular supercritical CO_2, as a solvent that exhibits even lower viscosity.

6 Measurements of T_1 and T_S in CO_2

6.1 Motivation

The increase in the lifetime of either T_1 or T_S is limited by the available viscosity range of organic solvents. The least viscous organic solvent we identified that could be obtained in deuterated form suitable for NMR experiments was diethyl ether, with a viscosity of 0.2 mPa*s. This is not much lower than the viscosity of acetone, which is at 0.34 mPa*s.

However, liquefied gases and supercritical fluids fortunately occupy a regime of viscosity an order of magnitude lower than common solvents. For subsequent experiments, we decided to work with CO_2, due to the fact that it is a substance that has been studied extensively, it has the ability to enter the supercritical regime, thus having unusual solvating properties and it is also non toxic.

6.2 High Pressure NMR Equipment

The manipulation of CO_2 in its liquid and supercritical form requires non-standard equipment. The condition to access the supercritical regime is 73.8 bar and 31.1 °C. For that reason, two identical High Pressure NMR Cells with Integrated Valve were purchased from Daedalus Innovations LLC (Aston, Pennsylvania, US).

The tubes comprising the NMR Cells are High Pressure Ceramic (Zirconia) NMR Tubes with an external diameter of 5 mm and an internal diameter of 3.6 mm. They can withstand pressures up to 1 kbar. For the filling of the NMR cells, a Filling Station was designed and constructed by Dr. Francesco Giustiniano, and is presented in Figure 9. An NMR Cell can also be seen within connected to the Filling Station within its containment module. The containment module is a blast box provided by the manufacturer and was integrated into the Filling Station. The custom made foam dewar (blue) used for CO_2 transfer into the NMR cell can also be seen in Figure 9.

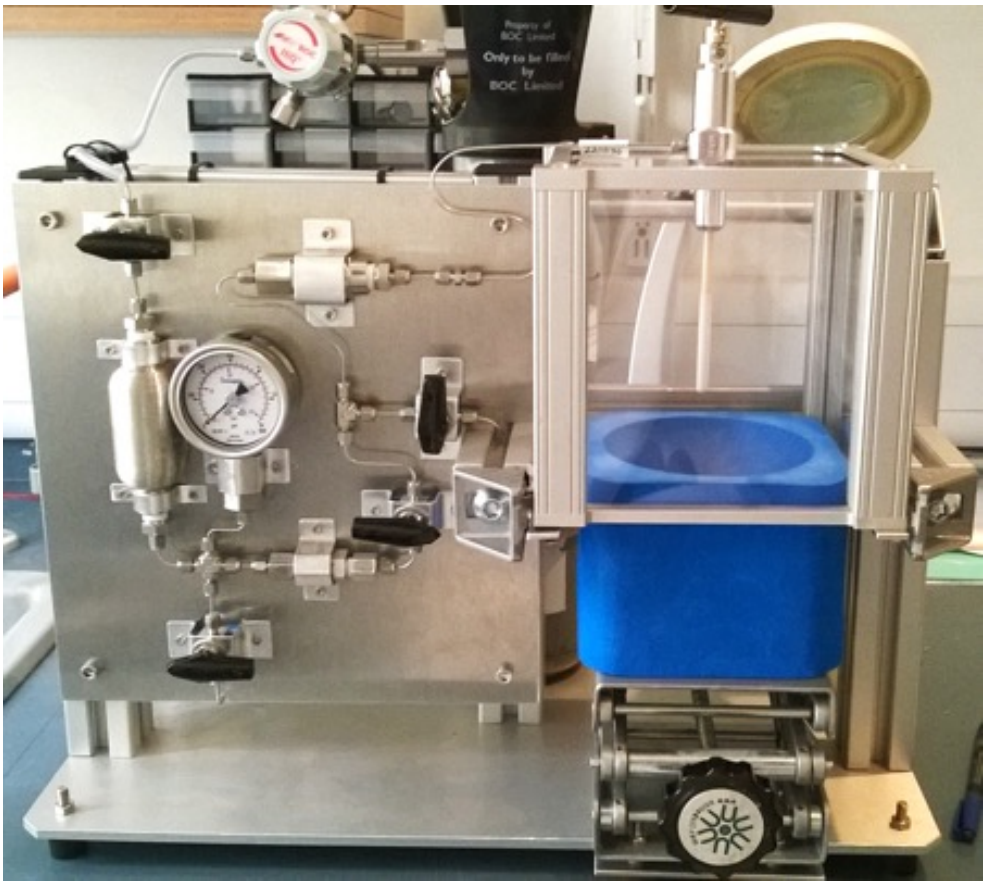

Figure 9: Custom made CO_2 Filling Station. Connected to the Filling Station is the NMR cell inside the containment module, above the custom made foam dewar (blue) used for the transfer of CO_2 by cooling down with liquid nitrogen.

A schematic representation of the Filling Station is depicted in Figure 10. The valves are denoted VA: VA1 is the valve that connects the CO_2 cylinder to the Filling Station, VA2 is the valve for venting, VA3 is the valve which leads to the NMR cell and VA4 is the valve which connects to the pump and for allows vacuum purging.

SV is the sampling vessel which is loaded with CO_2 to then be transferred in the NMR Cell. GA refers to the pressure gauge which indicates the pressure within the sampling vessel. BD stands for burst disk and it is a safety component of the Filling Station which can withstand up to 130 bar of pressure. At higher pressures it bursts in order to prevent damage to the other components of the Filling Station.

CV is a check valve which permits the flow of CO_2 from left to right only and prevents the CO_2 from returning to the sampling vessel.

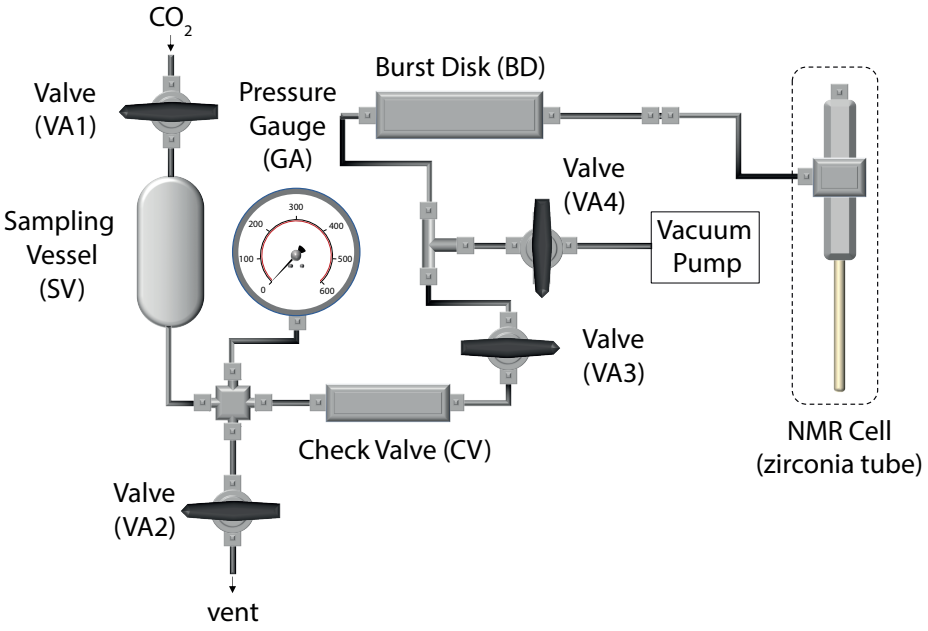

Figure 10: Schematic representation of the custom made CO_2 Filling Station. Connected to the Filling Station can be seen the NMR cell consisting of the 5 mm zirconia tube. The various valves are denoted VA, with VA1 being the valve that connects the CO_2 cylinder to the Filling Station, VA2 being the safety valve for venting, VA3 being the valve which leads to the NMR cell and VA4 the valve which connects to the pump and for allows vacuum purging. SV is the sampling vessel which is loaded with CO_2 and GA is the pressure gauge that indicates the pressure within the sampling vessel. BD is a safety element of the Filling Station, a burst disk that prevents damage to the other components of the Filling Station if the pressure were to exceed 130 bar. CV stands for check valve and its use is to prohibit the CO_2 from flowing from the NMR Cell to the sampling vessel.

6.3 Operating procedure of the Filling Station

The operating procedure of the Filling Station involves the following steps:

1. The compound under investigation is inserted in the tube and the cell is assembled.

2. The cell is connected to the Filling Station through the transfer line, that needs to be tightened in place.

3. The main valve of the CO_2 gas cylinder is opened, setting the target pressure on the gas regulator. The currently used regulator has a range 0-14 bar. This has proven to be a limitation and it is scheduled to be replaced with a gas regulator than can reach higher pressure values.

4. After the desired pressure has been set on the gas regulator, the sampling vessel (denoted SV in Figure 10) is filled by opening the valve VA1. The filling of the sampling vessel is complete once the pressure gauge (GA) has an indication which agrees with the regulator.

5. By closing VA1 which comes prior to the sampling vessel, the CO_2 is trapped. In order to achieve that, one needs to ensure that VA2 (the vent valve) and VA3 (the valve which leads to the NMR Cell) are also both closed.

6. Opening VA3 which leads to the NMR Cell, the CO_2 is then distributed freely in all sections of the Filling Station and the pressure at the pressure gauge (GA) drops slightly.

7. The sampling vessel has a volume of 50 mL. The zirconia tubes have a volume of ∼900 uL. The exact measurements of the tubes are given in Table 9. As it is expected, the CO_2 does not transfer quantitatively into the NMR Cell spontaneously.

   The transfer into the cell becomes possible by submerging the NMR Cell into liquid nitrogen which is contained in the custom made foam dewar which can be seen in Figure 9 as a blue cube.

8. The CO_2 condenses in the NMR Cell and once the transfer is complete (i.e. when the pressure gauge (GA) shows the desired indication), the NMR cell is sealed off through its needle valve.

9. The sample is allowed to reach room temperature within the blast box provided by the manufacturer. In the High Pressure Cell User's Guide provided by Daedalus Innovations, it is explicitly stated that the NMR Cell should be allowed at least 15 minutes after filling prior to removal from the blast box in order to minimize the risk of explosion outside of it, or even worse, within the spectrometer.

10. In order to insert the NMR cell into the spectrometer, special chains provided by the manufacturer need to be attached on either side of the NMR Cell. The NMR Cell is then lowered from the top of the bore into the probe.

    Further information can be found in the relevant documentation, namely the High Pressure Cell User's Guide provided by Daedalus Innovations and the Filling Station User Manual and Risk Assessment, written by Dr. F. Giustiniano.

6.3.1 Vacuum Purging

An important step in the procedure of filling the high pressure NMR cell is vacuum purging. The presence of oxygen is detrimental to the lifetime of the singlet state, even at trace quantities. In order to try and remove the oxygen, in a procedure equivalent to degassing under nitrogen or argon flow as with the other samples, a vacuum purging takes place. The steps it consists of are:

1. The sampling vessel is loaded with CO_2 as described in Section 7.3, and the valves VA1, VA2 and VA3 are closed.
2. VA4, the valve which connects the Filling Station to the pump is opened and the pump is turned on. That puts the section of the Filling Station after VA3 and the NMR Cell under vacuum.
3. VA4 is closed, while leaving the pump on, and VA3 is opened, allowing CO_2 to flow in the regions that were under vacuum.
4. VA3 is closed and VA4 is opened again, re-establishing the vacuum. The reason for doing so is that the pump is not very powerful and the Filling Station is not designed to be under a strong vacuum. Therefore we assume that the molecular oxygen is not all removed completely on the first time vacuum is established. For that reason we allow CO_2 to mix with it and apply vacuum again.
5. Steps 3 and 4 are repeated for a minimum of three cycles.
6. The sampling vessel is loaded with CO_2 at the desired pressure and ready to fill the NMR Cell.

6.4 Pressurised Sample Preparation

This section describes the details of the samples prepared in NMR Cells with CO_2 as the solvent and gives information on the tubes and inserts used. For all of the samples prepared, the vacuum purging procedure described in Section 7.3.1 was followed.

6.4.1 Zirconia Tubes

Table 9 details the weight (g) and volume (μL) of the Zirconia tubes used in experiments.

Tube	**Weight (g)**	**Volume (μL)**
Zirconia A	6.7199	879
Zirconia B	6.4433	899

Table 9: Zirconia tube specifications, weight and free volume.

6.4.2 Substituted Unlabelled Naphthalene in CO_2

Information on the samples of **II** in CO_2 (Section 7.5) is given in Table 10, including the amount of **II**, the amount of CO_2 and the tube used.

Sample	**II (mg)**	**CO_2 (mmol)**	**Tube**
1	40.3	11	Zirconia A
2	10.4	13	Zirconia B

Table 10: Details of the samples prepared involving **II** in CO_2 listing the quantity of **II**, the amount of CO_2 in mmol and the tube used for the preparation of each sample.

6.4.3 Substituted Labelled Naphthalene in CO_2

Information on the samples of **I** in CO_2 (Section 7.6) is given in Table 11.

Sample	**I (mg)**	**CO_2 (mmol)**	**Tube**
3	41.2	11	Zirconia A

Table 11: Details of the sample prepared for the experiments in Section 7.6 involving **I** in CO_2 including: the amount of **I**, the amount of CO_2 and the tube used.

6.4.4 Inserts

Table 12 lists information on the inserts used for experiments (see Section 7.7) including the weight of the insert, the tube it is paired with and the free volume available in the tube after insertion of the insert. The pairing is always followed as described below.

Insert	Insert Weight (g)	Tube	Volume of tube with Insert (uL)
Insert a	1.2839	Zirconia A	295
Insert b	1.2454	Zirconia B	342

Table 12: Information on the inserts used for experiments, introduced in Section 7.7. The table lists the weight of each insert, the tube it is used with and the free volume available in the tube with the insert.

6.4.5 Concentration Experiments

The procedure followed in sample preparation for experiments where the concentration of **I** was varied is discussed here. These experiments took place in order to determine the impact the quantity of the compound used has on viscosity of liquid CO_2 and consequently the relaxation of the longitudinal and singlet order.

Procedure

- In order to minimize error due to uncertainty in weighing, since we were going to work with small quantities, 10.1 mg of **I** were dissolved in 1.00 mL of analytical grade acetone, thus preparing a stock solution.
- Of the stock solution, 100 μL were inserted directly into the Zirconia Tube B, which contained the insert 2c. (Sample 4)
- The rest of the stock solution was distributed into four vials of 200 μL and the remaining 100 μL were left unused.
- The preparation of each sample (Sample 5-8) in this series of experiments involved the re-dissolution of the contents of each vial with acetone and the addition of it into the Zirconia Tube B.
- Subsequently, the tube was left open for the acetone to evaporate fully and was afterwards filled with CO_2.

The details of the sample preparation are summarized in Table 13.

Sample	I (mg)	CO_2 (mmol)	Volume (μL)	Concentration (mM)
4	1.0	4	342	12
5	3.0	4	342	36
6	5.1	4	342	61
7	7.1	4	342	85
8	9.1	4	342	108

Table 13: Details of the Samples 4-8 prepared for concentration experiments involving **I** in CO_2. Each sample was prepared in the same tube with the same insert (Zirconia Tube B and Insert b). The CO_2 had a total available volume of 342 μL to occupy within the tube.

.

An extra sample is included in the series of the concentration experiments, which was however not prepared following the sample procedure: It was prepared as a stand-alone sample, in Zirconia Tube A with the Insert a. Its details are mentioned in Table 14. The amount of **I** mentioned was weighed directly into the tube.

Sample	I (mg)	CO_2 (mmol)	Volume (μL)	Concentration (mM)
9	10.4	4	295	114

Table 14: Details of Samples 9 of **I** in CO_2. The sample was prepared in the Zirconia Tube A with Insert a, specifications of which are give in Table 12. The CO_2 had a total available volume of 295 μL to occupy within the tube.

6.4.6 Substituted Acetylene in CO_2

Information on Sample 10 of **III** in CO_2 (Section 7.4) is given in Table 15.

Sample	I (mg)	CO_2 (mmol)	Tube
10	7.0	4	Zirconia A

Table 15: Details of the sample prepared for the experiments in Section 7.4 involving **III** in CO_2 including: the amount of **III**, the amount of CO_2 and the tube used for the experiments.

6.5 Preliminary Experiments on Substituted Unlabelled Naphthalene in CO_2

6.5.1 Motivation

The experiments conducted with **II** in carbon dioxide serve as a proof of concept for further work. As the unlabelled version of the compound cannot access the singlet state, it serves mainly as a less expensive option to test the solubility of the compound in CO_2 as well as set up the procedures and understand the challenges involved with working with liquid and supercritical CO_2. In order to observe the transition from liquid to supercritical, the temperature was increased in small steps of one or two degrees. All of the experiments in this section took place at 11.7 T, according to Table 1.

6.5.2 Observations

Sample 1

In Figure 11, a multiple display of ^{1}H spectra acquired between 25 °C and 40 °C is presented. The all of the peaks double between 25 °C and 34 °C. This event was attributed to the likely existence of a second phase within the tube. At 40 °C the spectrum assumes a different form, providing an indication as to where the transition point might be. The assignment of the peaks in Figure 11 was done using the supporting information of the paper which describes the synthesis of **II**. [32]

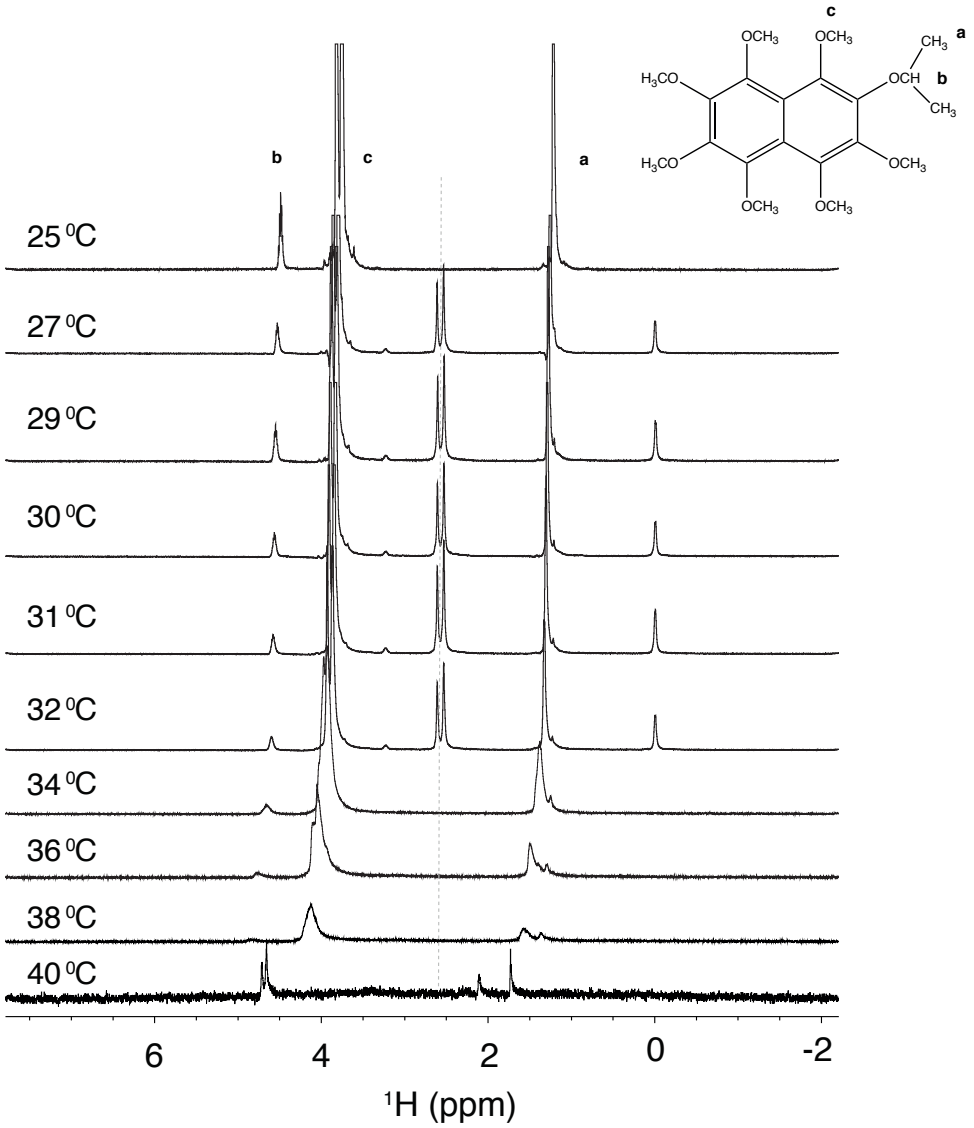

Figure 11: Multiple display of ^{1}H spectra from 25 °C to 40 °C of **II** in CO_2 (Sample 1). The sample is made as described in Table 10. The spectra were acquired at 11.7 T according to Table 1. The transition point appears to be between 38 °C - 40 °C.

In Figure 12, a multiple display of ^{13}C spectra acquired between 25 °C and 40 °C is presented. The peak observed belongs to CO_2. Since CO_2 is the solvent, it exists in such a quantity so that the natural abundance of ^{13}C makes is possible to observe and follow the signal. The indication on the transition point between liquid and supercritical phase is made more clear here. The transmitter is on resonance with the CO_2 peak (as well as in Figure 14, as it is the only peak appearing on the spectra and has been referenced as point 0 in the ppm scale.

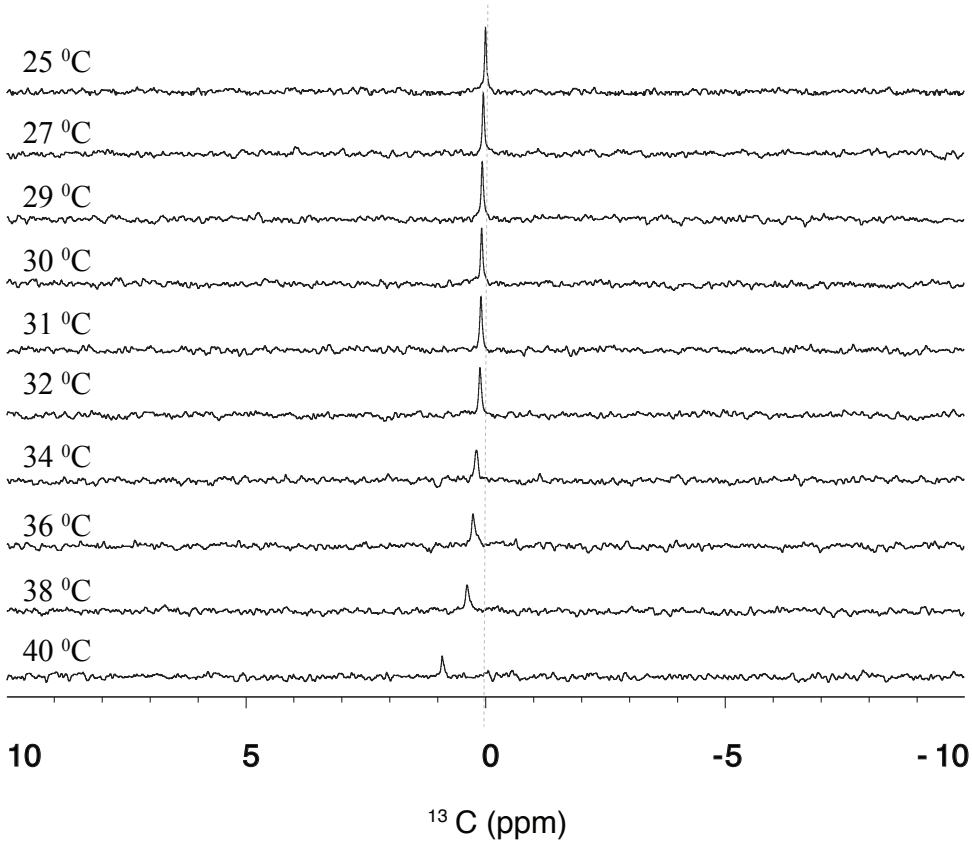

Figure 12: Multiple display of ^{13}C spectra from 25 °C to 40 °C of **II** in CO_2 (Sample 1). The sample is made as described in Table 10. The spectra were acquired at 11.7 T according to Table 1. The transition point from liquid to supercritical phase appears to be between 38 °C - 40 °C. The transmitter is on resonance with the CO_2 peak, as it is the only peak appearing on the spectra and has been referenced as point 0 in the ppm scale.

Sample 2

The investigation conducted on Sample 2 was more thorough and a larger number of temperatures were explored. Figure 13 consists of a multiple display of ^1H spectra from 23 °C to 40 °C for Sample 2 of **II** in CO_2. The ^1H spectra of Sample 2 appear to be free from extra peaks. This is attributed to the smaller quantity of compound and the larger quantity of CO_2 (compared to Sample 1) used for the preparation of the sample as described in Table 10.

The other interesting observation in Figure 13 is that the transition point between the liquid and supercritical phase appears to be at around 38 °C. The same observation is evident in Figure 14 as well, where a multiple display of ^{13}C spectra from 23 °C to 40 °C of **II** in CO_2 (Sample 2) is presented. This observation could be related to the lower quantity of compound **II** in CO_2. It is speculated that the quantity of the compound has an impact on the exact position of the critical point, since CO_2 is no longer pure.

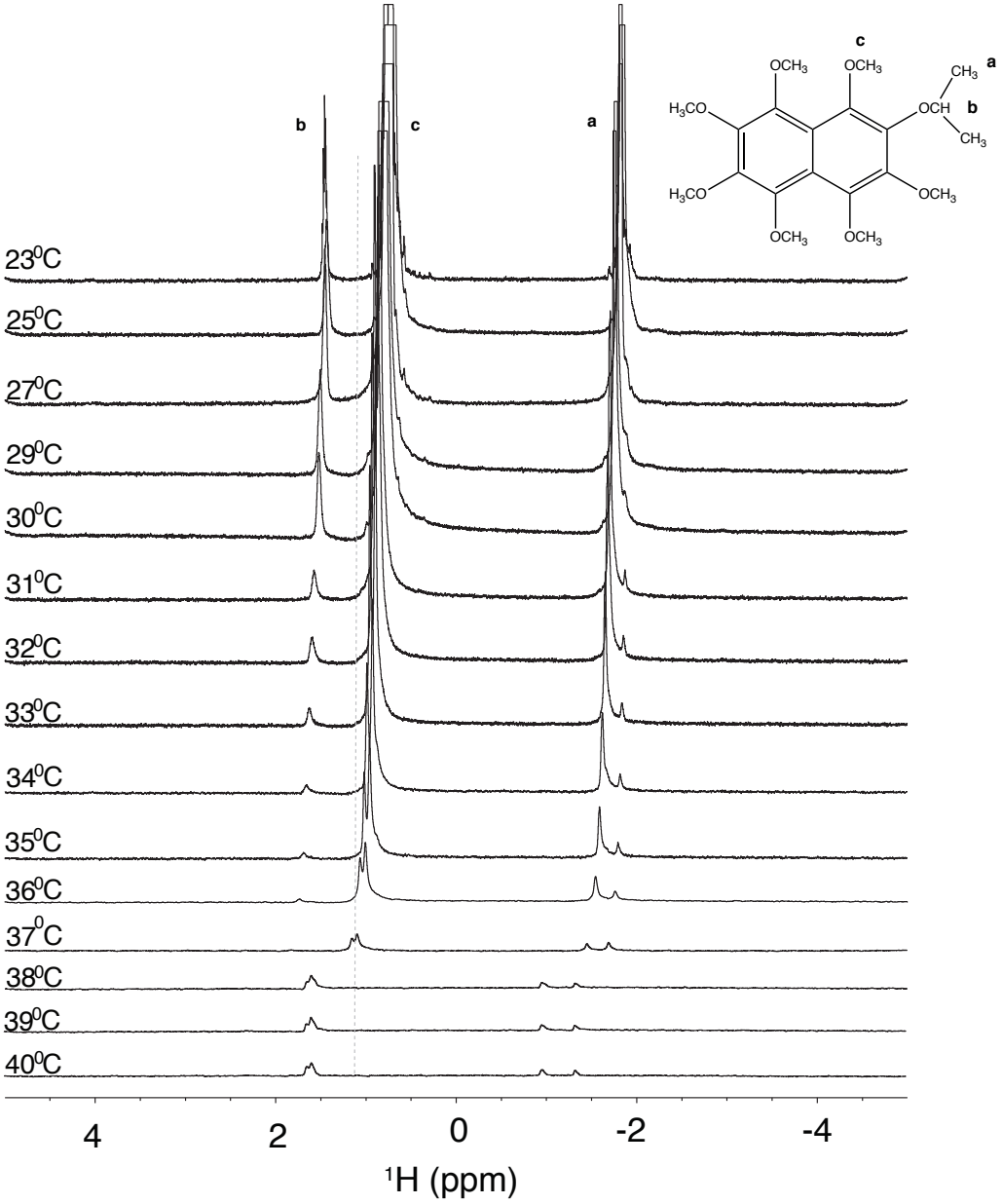

Figure 13: Multiple display of ^{1}H spectra from 23 °C to 40 °C of **II** in CO_2 (Sample 2). The spectra were acquired at 11.7 T according to Table 1. The sample preparation was done according to Table 10. The transition point between the liquid and supercritical phase appears to be between 37 °C and 38 °C.

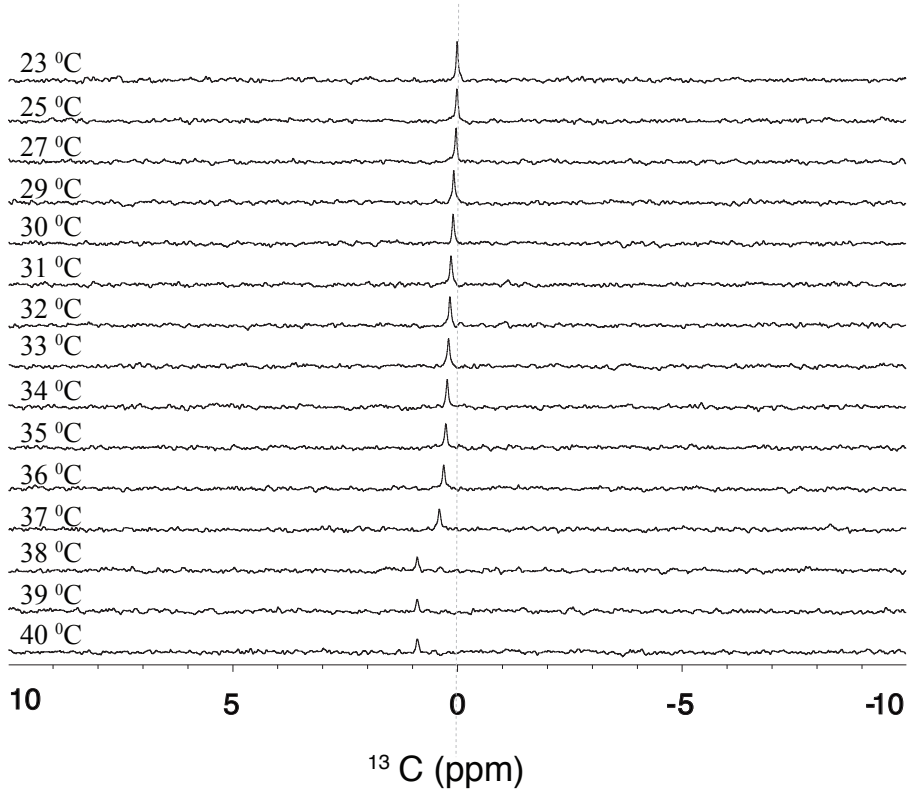

Figure 14: Multiple display of ^{13}C spectra from 23 °C to 40 °C of **II** in CO_2 (Sample 2). The sample is made as described in Table 10. Measurements were performed at 11.7 T as described in Table 1. The transition point between the liquid and supercritical phase appears to be between 37 °C and 38 °C.The transmitter is on resonance with the CO_2 peak, as it is the only peak appearing on the spectra and has been referenced as point 0 in the ppm scale.

6.5.3 Discussion

With this set of experiments we have established that acquisition of ^{1}H spectra of **II** in both liquid and supercritical CO_2 is possible, as well as ^{13}C spectra of the CO_2.

An increase in temperature contributes to resolution deterioration, leading to loss of fine structure and loss of signal intensity. Reduction in temperature and re-acquisition (which are not presented here) restore the original spectrum.

One of the most important observations made while acquiring preliminary data was that there is a lag between the stabilization of the sensor at each temperature and the actual equilibration of the sample. For that reason, great care was taken in order to allow sufficient time (a minimum of 30 minutes) to elapse between setting the temperature on a value and acquiring data.

Extra peaks appear between 25 °C and 36 °C for Sample 1 but not for Sample 2. It is highly likely that in the case of Sample 1, there was a secondary phase forming. Reducing the mass of the compound and increasing the solvent appears to resolve this,

which is an indication of a concentration sensitivity of the system.

The transition from the liquid to the supercritical phase is happening as indicated by the sudden jump in chemical shifts as well as the change of the peak shapes in the case of the ^{1}H spectra. It is known that the critical point for pure CO_2 is at exactly 31°C and 73.8 bar. However, we see that for both Samples 1 and 2, the temperature at which the transition is observed is higher than the critical temperature. We appoint that to the fact that our experiments involve a system between the compound (**II**) and CO_2, rather than pure CO_2. Therefore, it is expected that the transition point is shifted.

For Sample 1 the transition appears to be at around 40 °C but for Sample 2 it is at around 38°C. The reason for this is suspected to be again the difference in concentrations between the two samples. It appears that the more compound is dissolved in CO_2, the further the transition point is shifted. This poses further evidence towards a concentration dependence on the behavior of the samples.

At each temperature mentioned above, T_1 measurements were performed on the ^{1}H. Of those, only the ones relevant to the CH (denoted **b**) signal are reported. The results, given in Table 16 do not seem to agree between the two measurements. Again we suspect that the discrepancies between the measurements could be caused because of the differences in concentration.

	Sample 1	**Sample 2**
T (°C)	**T_1 (s)**	**T_S (s)**
22		7 ± 1
25	7.8 ± 0.3	7.1 ± 0.6
27	7.9 ± 0.4	8.5 ± 0.2
29	8.8 ± 0.3	7.4 ± 0.2
30	8.8 ± 0.3	9.3 ± 0.3
31	10.2 ± 0.2	11.2 ± 0.7
32	11.4 ± 0.2	15 ± 1
33		19 ± 2
34	13.1 ± 0.6	18 ± 2
35		14.1 ± 0.7
36	18 ± 2	12.2 ± 0.9
37		16 ± 2
38	22 ± 6	12 ± 2
39		16 ± 3
40		7 ± 2

Table 16: T_1 values and corresponding fitting error calculated with Mathematica for the -CH proton of **II** in CO_2. Comparison between Sample 1 and Sample 2 of **II** for temperatures ranging from 22°C to 40°C

6.5.4 Conclusions

Compound **II** appears to be soluble in both liquid and supercritical CO_2 which is encouraging since the labelled, deuterated version of the Naphthalene, **I**, is expected to behave in the same way. The supercritical regime is accessed and data can be collected. Increase in temperature and crossing into the supercritical regime do not have permanent effects on the compound.

The presence of the compound in the CO_2 causes a shift of the transition point between liquid and supercritical phase, dependent on the concentration of the sample. This is a point that merits further investigation in order to identify the optimal conditions to work with. There is also strong evidence that the outcomes of the measurements are sensitive to the concentration of the sample (Table 16).

6.6 Preliminary Experiments on Substituted Labelled Naphthalene in CO_2

6.6.1 Motivation

This section discusses the preliminary experiments conducted on **I** in liquid and supercritical CO_2 in order to measure T_1 and T_S values. The sample preparation was done according to Table 11 and the measurements were conducted at 11.7 T according to Table 1.

6.6.2 Observations

Figure 15 presents a multiple display of ^{13}C spectra of **I** in CO_2 (Sample 3) for a range of temperatures between 25 °C and 45 °C. The temperatures explored in this section were fewer compared to the ones in the case of **II**, in order to keep the experimental times reasonable as carbon nuclei relax more slowly than protons.

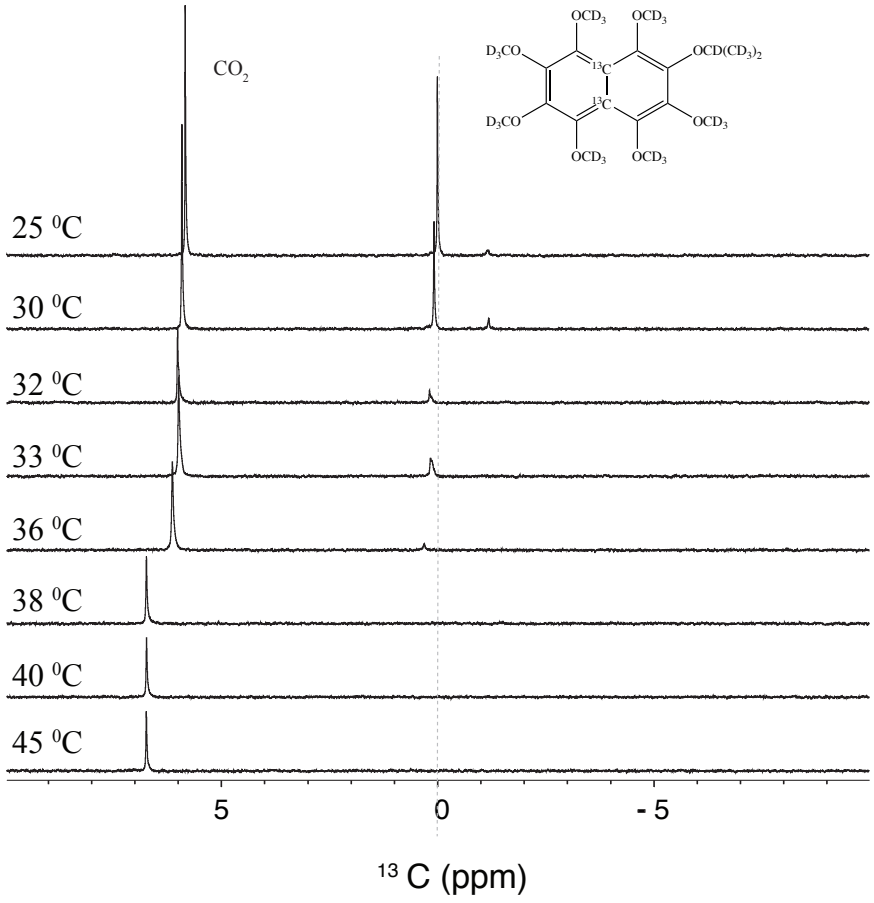

Figure 15: Multiple display of ^{13}C spectra of **I** in CO_2 for a range of temperatures between 25 °C and 45 °C. The sample was prepared according to Table 11 and the measurements were conducted as described in Table 1. The transmitter is on resonance with the peak which belongs to **I**, as it is the peak on interest and has been referenced as point 0 in the ppm scale.

The two ^{13}C atoms of **I** appear as a single peak, as can be seen in Figure 15. This is of course due to the fact that the chemical shift difference between the two sites is a lot smaller than their J-coupling. Between 36 °C and 38 °C, the Naphthalene peak vanishes while at the same time the CO_2 peak exhibits a sudden jump in chemical shift, indicating the transition point.

The results of the measurements of T_1 on ^{13}C for both the CO_2 and **I** are presented in Table 17. In Figure 15 there is an extra ^{13}C peak appearing at 25 °C which does not appear in the saturation recovery experiment. It appears at 30 °C and 32 °C, making T_1 measurements possible at those temperatures, even though the peak is not visible at 32 °C in Figure 15.

T (°C)	**T_1 of ^{13}C (s)**		
	CO_2	**I**	**Extra Peak**
25	9.1 ± 0.5	18.2 ± 0.9	—
30	8.4 ± 0.3	17.8 ± 0.6	5.0 ± 0.7
32	10.8 ± 0.2	21.9 ± 0.5	3.7 ± 0.5
33	10.1 ± 0.1	36 ± 4	—
36	8.0 ± 0.1	38 ± 13	—
Phase Transition			
38	3.8 ± 0.4	—	—
39	3.6 ± 0.3	—	—
40	3.4 ± 0.2	—	—

Table 17: T_1 of ^{13}C values and corresponding fitting error calculated in Mathematica for CO_2, **I** in CO_2 and an unidentified extra peak, over a range of temperatures between 25 °C and 40 °C. The sample preparation (Sample 3) was done according to Table 11 and the measurements were conducted at 11.7 T according to Table 1.

6.6.3 Discussion

An increase in temperature brings deterioration of the signal to noise ratio. The ^{13}C peak of **I** is barely distinguishable from the noise at 36 °C, which results to a very poor fit. All fits concerning the extra peak are rather poor as well.

The transition from the liquid to the supercritical phase appears to be occurring between 36 °C and 38 °C. However, after the phase transition the Naphthalene peak disappears and it is impossible to take measurements. This is not because of saturation of the signal due to fast pulsing. The saturation recovery experiment inherently circumvents the need for a recycle delay of 5 times T_1. Still, the saturation recovery experiments conducted gave meaningless results. We attribute this phenomenon to fast convection of **I** in and out of the active coil region. After the phase transition we observe that the CO_2 peak relaxes much faster than it did in the liquid phase.

A T_S measurement took place at 25 °C and the singlet decay curve as a function of time is presented in Figure 16. It appears that the singlet decays with two different rates, one of which is very fast. The two components, as calculated with Mathematica are: 2.7 ± 0.2 and 475 ± 31.

There were no attempts made for T_S measurements at 30 °C and 32 °C in order to save time. At 33 °C and 36 °C it was impossible to find the conditions for the transfer of longitudinal magnetization to singlet. In particular, the τ_j optimization would not converge into a single value. Above the transition point there was no ^{13}C peak to measure on.

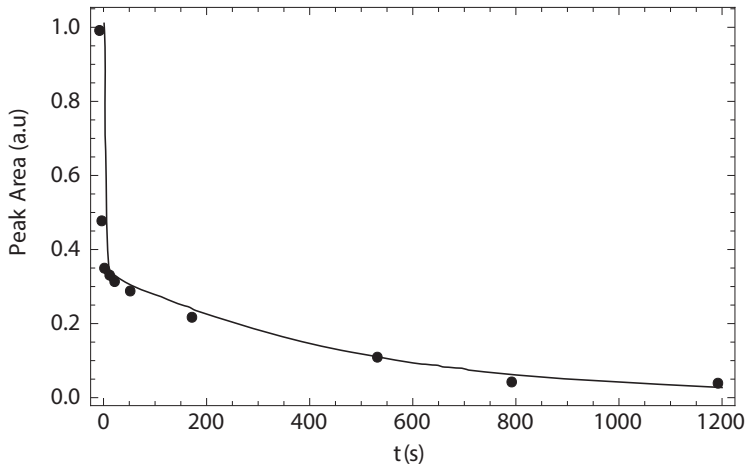

Figure 16: Singlet order decay curve fit as a function of time at 25 °C for Sample 3. The decay is biexponential instead of monoexponential and the two components, as calculated with Mathematica are: 2.7 ± 0.2 and 475 ± 31.

6.6.4 Conclusions

The two component decay of the singlet is an unfortunate complication that led to a reduced observed T_S. Liquid and supercritical CO_2 both exhibit low viscosity values. The NMR Cell consists of a metal valve which could cause a temperature gradient along the axis of the tube. For those reasons, we suspected that the fast element in the decay of the signal would be caused by convection.

A common solution to combat convection is spinning of the sample, however this is not an option because the tube is pressurized and the NMR Cell has a heavy metal valve on top of it. The decision was made to try and restrict the sample within the active area of the detection coil in order to reduce convection.

Since measurements in liquid CO_2 are not restricted by solubility, we decided we would not complicate matters for the time being by trying to cross into the supercritical regime. For that reason the following sections refer exclusively to liquid CO_2 unless explicitly stated otherwise.

6.7 Sample Restriction within the Active Coil Region by Inserts

6.7.1 Motivation

In an attempt to restrict the sample volume within the active coil region and reduce the effects of convection, extensive work was done on the design of an appropriate insert. A selection of some of the inserts designed and manufactured is presented in Figure 17. From left to right they are depicted as follows: 1. Glass insert with a "boat", 2. PCTFE insert with a ring cavity and a "boat", 3. PCTFE insert with a ring cavity and a "chamber", 4. PCTFE insert with a "chamber", 5. Glass insert with a "chamber" and a PCTFE cap.

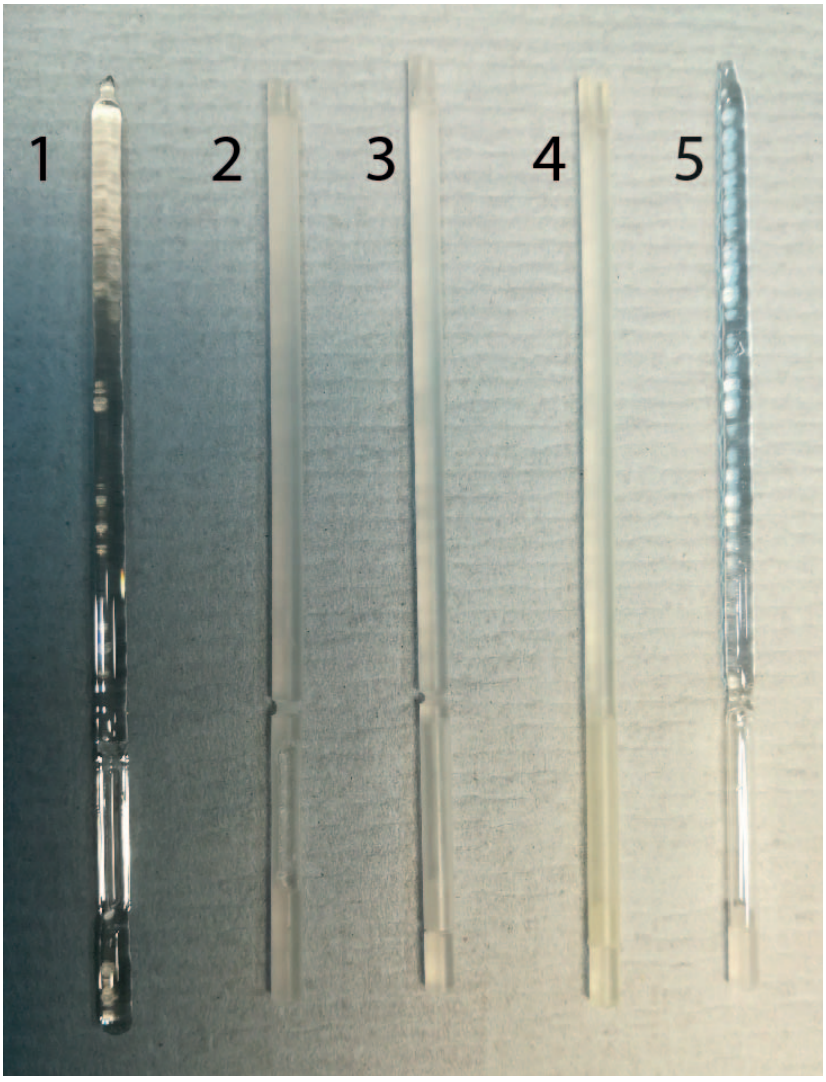

Figure 17: A selection of inserts designed for restricting the sample volume within the active coil region in order to reduce the effects of convection in the measurements. From left to right: 1. Glass insert with a "boat", 2. PCTFE insert with an o-ring cavity and a "boat", 3. PCTFE insert with an o-ring cavity and a "chamber", 4. PCTFE insert with a "chamber", 5. Glass insert with a "chamber" and a PCTFE cap.

A schematic representation of the inserts shown in Figure 17 can be seen in Figure 18 below.

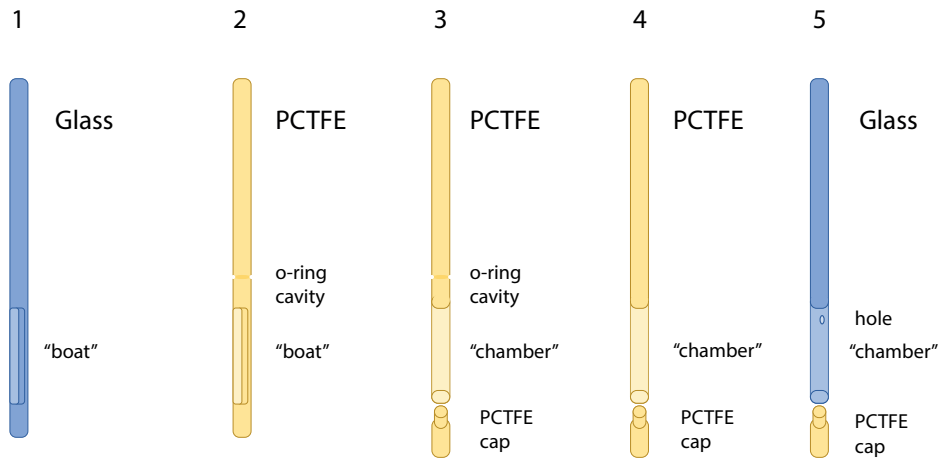

Figure 18: A schematic representation of the inserts shown in Figure 17 selection of inserts designed for restricting the sample volume within the active coil region in order to reduce the effects of convection in the measurements.

A variety of designs was tested in order to identify the optimum. The material used was either glass or PCTFE (Polychlorotrifluoroethylene) purchased by Goodfellow. The glass inserts were manufactured by the Glassblowing Workshop in Chemistry while the PCTFE ones were manufactured by Dr. Francesco Giustiniano.

In order to restrict the sample, three designs were tried: a. "boat" type insert, where the insert consists of a rod of material in which a boat shaped cavity is carved at the height of the coil, b. "chamber" type inserts, where the insert is a rod that has a chamber shaped cavity at the bottom part of the insert, which is closed with a cap and c. either "boat" or "chamber" type inserts that also have a ring cavity. The idea behind the last design was to insert an o-ring in order to restrict motion further, but those inserts were never used with an o-ring. The reason for this is that by then it was clear that the glass inserts were superior to the plastic ones and it was not possible to manufacture a glass insert with an o-ring cavity.

6.7.2 Discussion

The criteria according to which the final selection of insert was done were the following: monoexponential decay of the singlet lifetime, longest observable value of lifetime and no signs of chemical alteration of the compound under study.

The PCTFE design repeatedly gave shorter than optimal lifetimes. Furthermore, without exception whenever this material was used, while compound **I** has the form of white powder, at the end of the experiment a yellow oil was remaining in the tube. We believe this is probably due to impurities attached to the material and we decided not to pursue this line of research anymore.

The "chamber" type of inserts formed a bubble of gaseous CO_2 at the top part of the chamber if the sample had to be heated (e.g. for the compound to dissolve in CO_2 faster). In the case that the condensation process of the CO_2 within the tube generated a bubble, there was no way to remove it afterwards. The reason why this poses an inconvenience is that the bubble tends to expand into the active coil region, interfering with the measurements. The bubble would displace the solution from the active coil region, reducing sensitivity and in many cases eliminating the signal altogether.

The zirconia tubes are not transparent. The reason why we are aware of this issue is because the inserts were also tried in transparent sapphire tubes as well. The sapphire tubes are of lower quality and can only withstand pressures up to 100 bar and were therefore deemed precarious to insert in an NMR spectrometer. No actual experiments were performed with them.

It was found that by making a small hole at the top of the insert this issue of the bubble formation is eliminated. It is important for the glass to be treated properly otherwise the hole consists of a structural weakness and the insert breaks. It is easy to track whether the insert is intact while measuring, as the decay curve becomes biexponential the moment the insert breaks.

Despite the progress with the "chamber" type inserts, the lifetimes observed with them still remained lower than the maximum measured values. This might be connected to the fact that the caps used with those type of inserts are made from PTCFE. Since it was extremely difficult to produce a glass cap small enough to match the "chamber" type inserts properly, and the fact that the zirconia tubes are not transparent, we decided to purchase a high quality 10 mm sapphire NMR cell from Daedalus Innovations LCC and to manufacture a glass "chamber" type insert with a glass cap. This can be seen in Figure 19.

Various modifications need to take place on the Filling Station to be able to accommodate the 10mm tube but preliminary tests have proven to be very promising. This will involve future work in the group and will not be discussed further here.

6.7.3 Conclusions

The best results to this date according to the criteria listed above (preservation of compound, monoexponential decay of the lifetime against time and longest value of lifetime possible) were the ones obtained by the use of glass inserts with a boat, such as **1** depicted in Figure 17. The results discussed in the following sections concern only this particular type of insert and we will not present results obtained with any of the others.

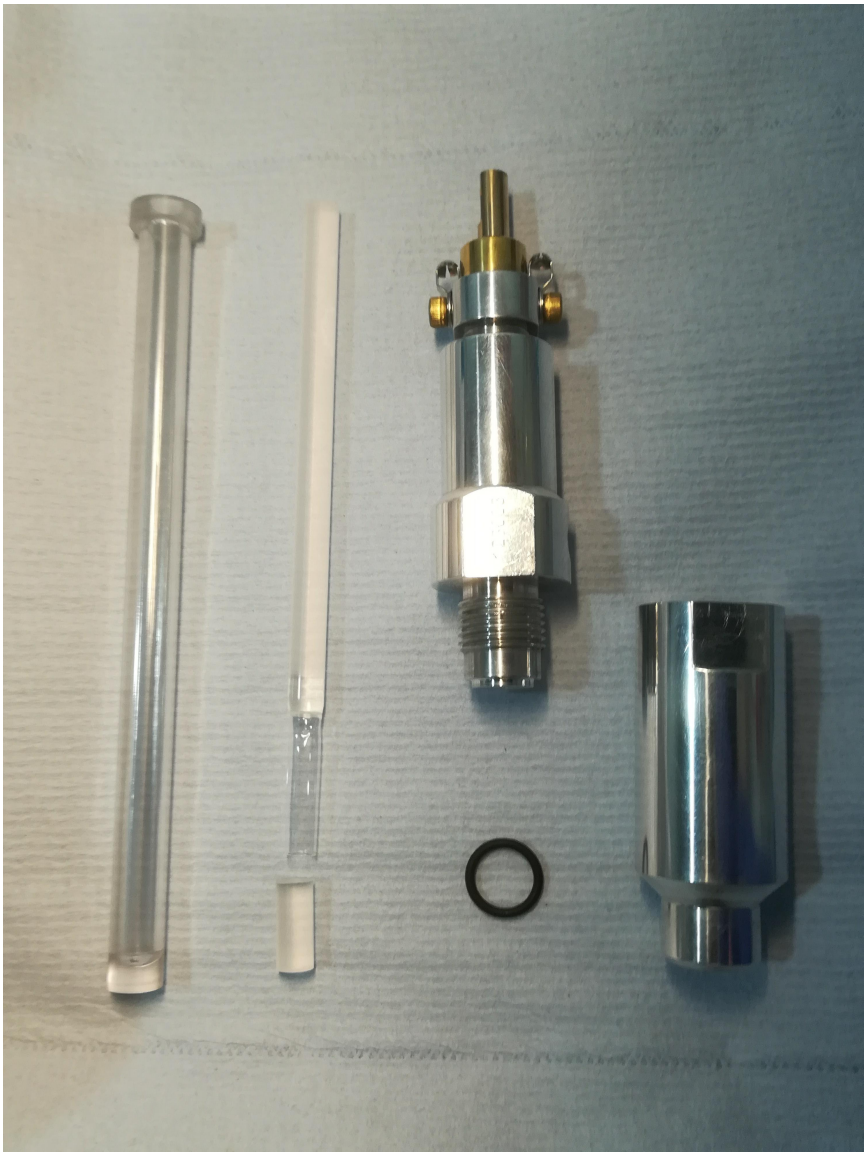

Figure 19: The 10mm NMR cell purchased by Daedalus Innovations LCC disassembled along with the 10mm glass "chamber" type insert and its glass cap.

7 Measurements of T_1 and T_S in CO_2 with a Glass Insert

The glass insert that can be seen in Figure 20 was manufactured by the Mechanical Workshop in Chemistry, used in order to restrain the volume of the sample, hoping that it will eliminate the relaxation element that was speculated to correspond to convection. Sections 7.1 - 7.3 refer to experiments using **I** while Section 7.4 concerns **III**.

Figure 20: The NMR cell disassembled along with a zirconia tube (Zirconia A) and a "boat" type glass insert (Insert a). In order to assemble the cell, the insert goes into the tube and then the tube is inserted into the small part of the valve. The o-ring is placed on top of the tube before the bigger part of the valve so that it is not in direct contact with the tube.

7.1 Concentration Experiments

7.1.1 Motivation

In previous experiments there were indications that the quantity of the compound in CO_2 affects the results of the measurements. Liquid CO_2 is a solvent of extremely low viscosity. It has an η value of 0.06 mPa/s at 75 bar and 298 K. (The critical point is at 73.9 bar and 304.25 K). [3] It is possible that the mere act of dissolving a compound in it (in this case **I**), potentially changes (increases) the viscosity.

The experiments described in this section took place in order to verify this hypothesis and to determine the measure of change of T_1 and T_S values with increasing viscosity. Diffusion coefficient measurements were conducted in order to determine the viscosity of CO_2, using the diffusion coefficient of **I** in deuterated methanol as a reference point. All experiments in this section were conducted at 16.4 T according to Table 1.

7.1.2 Discussion

T_1, T_S and diffusion coefficient measurements were performed on Samples 4-9 at 16.4 T according to Table 1. The results of this set of experiments are presented in Table 18.

The conditions that apply to the preparation of Sample 9 do not match the rest of the Samples 4-8. The tube and the insert used are different. Details of the sample preparation are given in Tables 13 and 14. For that reason we will refer to the concentration of the samples from now on instead of the amount of **I** used. In order to proceed with the comparison we need to make the assumption that the CO_2 occupies the entire available volume of the tube.

Sample	**Concentration (mM)**	**T_1 (s)**	**T_S (s)**	**D *10^{-9} (m^2/s)**
4	12	-	-	-
5	36	20.5 ± 0.2	505 ± 25	9.0 ± 0.2
6	61	21.4 ± 0.3	433 ± 19	8.9 ± 0.2
7	85	19.1 ± 0.1	525 ± 23	8.7 ± 0.07
8	108	17.6 ± 0.1	513 ± 15	7.7 ± 0.05
9	114	12.9 ± 0.3	297 ± 19	3.9 ± 0.06
Methanol		4.17 ± 0.03	92.0 ± 0.9	1.1 ± 0.005

Table 18: T_1, T_S and diffusion coefficient values measured for Samples 4-9 of **I** in CO_2. Samples 4-8 are prepared as described in Table 13, while Sample 9 is prepared as described in Table 14 The T_1 and T_S values of **I** in methanol are the ones presented in Table 5. The results of **I** in methanol are used for reference.

- Sample 4 gave a detectable signal that was however too weak to give meaningful results. The poor signal to noise ratio prevented quantification in this case. This sample will not be mentioned further.
- Sample 6 is introduced only for reasons of completion and in order to point out how important equilibration of the samples is. By equilibration we mean leaving the sample both reach room temperature and rest after the filling is complete. Since liquid nitrogen is used to condense CO_2 in the zirconia tube, the NMR cell is cold and needs to reach room temperature. However, as was discovered, this is not enough for the compound to fully dissolve in it, resulting in misleading values.

This conclusion was reached by measuring the samples on the day they were prepared and some days after preparation. Sample 6 is depicted in Figures 21 and 22 in order to demonstrate that, but is excluded from any further discussion.

- The diffusion coefficient of **I** in deuterated methanol was measured in order to provide a reference point for the measurements in CO_2. The T_1 and T_S values presented in Table 18 are the same values presented in Table 5.

Figure 21 presents the T_1 and T_S values of **I** plotted against the concentration of **I** in CO_2 at 16.4 T, while Figure 22 shows the diffusion coefficient plotted against the concentration of **I** in CO_2 at 16.4 T. Sample 6 is coloured red in order to demonstrate that it is an outlier. Samples 5-9 were prepared according to Tables 13 and 14.

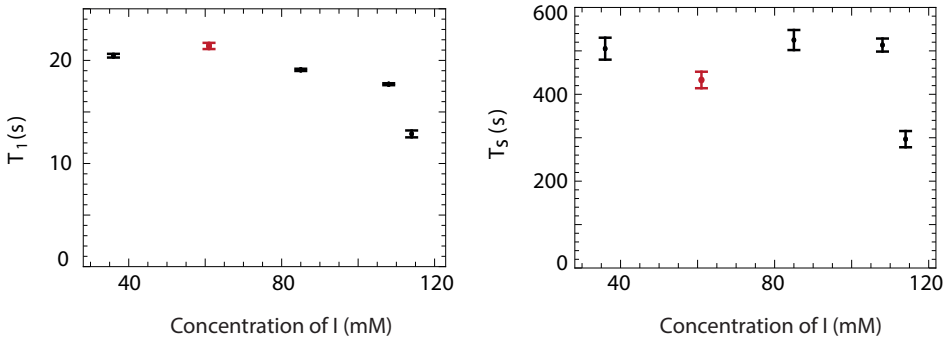

Figure 21: T_1 and T_S values of **I** plotted against the concentration of **I** in CO_2 at 16.4 T. The value corresponding to 61 mM of **I** is an outlier (coloured red) since Sample 6 had not equilibrated properly prior to measurements. The preparation of the samples can be found in Tables 13 and 14.

While for T_1 and diffusion coefficient values the decrease with increasing concentration is evident, it is easy to observe that the T_S values remain practically invariant until a large drop in Sample 9. This shows that in the range of 36-108 mM the T_S remains invariant with increasing concentration of **I**. This is an interesting, counter-intuitive finding. In order to put the results into context, we will calculate the viscosity of CO_2 from the diffusion coefficient values.

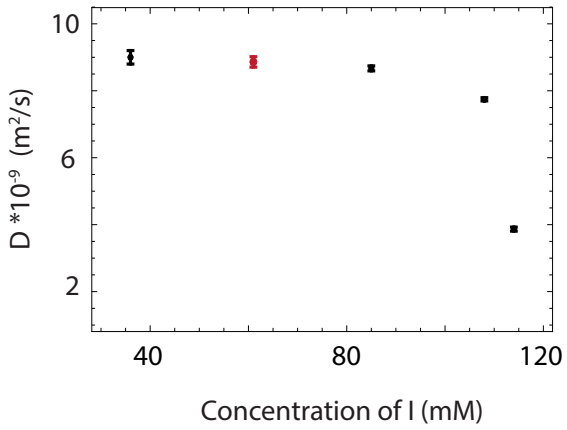

Figure 22: Diffusion coefficient values of **I** plotted against the concentration of **I** in CO_2 at 16.4 T. The value corresponding to 61mM of **I** (coloured red) is an outlier since Sample 6 had not equilibrated properly prior to measurements. The samples were prepared according to Tables 13 and 14.

7.1.3 Viscosity Calculation

In order to proceed with the calculation of viscosity from the diffusion coefficient measurement conducted, we are making a number of assumptions. Assuming that we are in a regime where the Stokes-Einstein equation (Eq. 20) holds even though the molecule under discussion is not perfectly spherical, and that the hydrodynamic radius of **I** is identical in MeOD and liquid CO_2, then we have:

$$D = \frac{k_B T}{6\pi\eta r} \tag{21}$$

Where:

- D is the diffusion coefficient of the compound
- k_B is Boltzmann's constant
- T is the absolute temperature
- η is the dynamic viscosity of the solvent
- r is the radius of the spherical particle

Therefore, having measured at the same temperature (295K) we have:

$$\frac{D_{CO_2}}{D_{MeOD}} = \frac{\eta_{MeOD}}{\eta_{CO_2}} \tag{22}$$

Assuming the viscosity value for deuterated methanol in our system does not significantly deviate from that found in the literature, then we have η_{MeOD}=0.52. Rearranging gives:

$$\eta_{CO_2} = \eta_{MeOD} \frac{D_{MeOD}}{D_{CO_2}} \tag{23}$$

And this allows us to calculate the viscosity values for CO_2 samples. The results are shown in Table 19.

Sample	**Concentration (mM)**	T_1 **(s)**	T_S **(s)**	**D *10^{-9} (m^2/s)**	η **(mPa*s)**
5	36	20.5 ± 0.2	505 ± 25	9.0 ± 0.2	0.07
7	85	19.1 ± 0.1	525 ± 23	8.7 ± 0.07	0.07
8	108	17.6 ± 0.1	513 ± 15	7.7 ± 0.05	0.08
9	114	12.9 ± 0.3	297 ± 19	3.9 ± 0.06	0.15
Methanol		4.17 ± 0.03	92.0 ± 0.9	2.1 ± 0.03	0.52*

Table 19: T_1, T_S and diffusion coefficient values measured for Samples 5-9 of **I** in CO_2, prepared as described in Tables 13 and 14. The T_1 and T_S values of **I** in methanol are the ones presented in Table 5. The results of **I** in methanol are used for reference. *The value of the viscosity of **I** in methanol is the one found in literature[1]The and has not been calculated.

In order to validate this method of calculating the viscosity of CO_2, the diffusion coefficient of **I** in acetone, which has a known viscosity of 0.34 mPa*s according to literature, was measured. The viscosity was then calculated based on the diffusion coefficient of methanol and the viscosity of methanol as found in literature. The results are presented in Table 20 below. There is good agreement between the literature and experimental values if one also considers that the literature value refers to 20 °C, while our measurements take place at 295 K (22 °C), where the viscosity is expected to be lower.

Sample	**D *10^{-9}(m^2/s)**	**Literature** η **(mPa*s)**	**Experimental** η **(mPa*s)**
Methanol	2.1 ± 0.03	0.52	-
Acetone	1.1 ± 0.005	0.34	0.29

Table 20: Diffusion coefficient values measured at 16.4 T for **I** in deuterated methanol and acetone, prepared as described in Table 3. We compare the experimental value of viscosity of acetone calculated from the diffusion coefficients and the viscosity value of MeOD as found in literature.

As we can observe in Table 19 there is a jump in the viscosity values between Sample 8 and Sample 9 which corresponds to the jump between the T_S values. The reason why the viscosity changes so much between 108 and 114 mM is not known.

As described in Equation 11, T_1 and T_S are inversely proportional to η.

$$\frac{1}{T_1, T_S} = R_1, R_S \propto \tau_c \propto \eta$$

Therefore :

$$\frac{T_{S,CO2}}{T_{S,MeOD}} = \frac{\eta_{MeOD}}{\eta_{CO2}} \tag{24}$$

- Calculating the ratio between the viscosity of methanol and that of CO_2, (right part of Equation 24) gives us the maximum expected ratio between the T_S values.
- Calculating the ratio between the T_S values of CO_2 and that of methanol, (left part of Equation 24) gives us the observed experimental ratio between the T_S values.
- By dividing the "T_S ratio" with the "η ratio" we calculate the factor we have over the theoretical value expected.

In Table 21, we calculated the ratio between the viscosity values (MeOD/CO_2), that we call the "η ratio" using the literature value for **I** in MeOD (0.52 mPa*s) and the values calculated for CO_2 from the diffusion coefficient in Table 19. We also calculated the ratio between the T_S values (CO_2/MeOD), which we call "T_S ratio",using the values measured.

Sample	η **(mPa*s)**	T_S **(s)**	T_S **ratio**	η **ratio**	**Ts extension compared to the theoretical maximum* (%)**
5	0.07	505 ± 25	5.5	7.9	70
7	0.07	525 ± 23	5.7	7.6	75
8	0.08	513 ± 15	5.6	6.8	83
9	0.15	297 ± 19	3.2	3.4	95

Table 21: Presentation of the calculated viscosity values of Samples 5-9, their T_S values as measured at 16.4 T, the T_S ratio between the T_S values of CO_2/MeOD, the η ratio between the viscosity values of MeOD/CO_2, which gives the theoretical maximum of the previous value and the percentage of T_S extension compared to the theoretical maximum*.
*this is based on viscosity values calculated from diffusion experiments and assuming **I** is spherical and has identical hydrodynamic radii in both MeOD and liquid CO_2 as well as that for the viscosity of MeOD, the value does not deviate from the one found in literature (0.52 mPa*s).

7.1.4 Conclusions

Sample equilibration takes a long time and it can interfere with the results obtained. One must ensure that the sample has had enough time to equilibrate and prepare it some days in advance. The matter might merit from further investigation in order to identify the minimum time one can allow for equilibration.

While T_1 and D values decrease slowly with the increase of the concentration, the T_S remains effectively unaffected in the range between 20 and 60 mM. This is a very important conclusion. Working with the maximum concentration possible allows for a better signal to noise ratio with effectively no impact on the T_S, which is of crucial importance when it comes to measurements in lower magnetic fields.

As can be observed in Table 21, the lower the viscosity, the further away the values deviate from the theoretical maximum that could be achieved. This implies that there is an upper limit as to how the T_S can be extended by lowering the viscosity. This will be made more clear in the following section.

7.2 Field Study

Since in the range of 36-108 mM of **I**, the T_S values remain practically invariable, Sample 8 was deemed an appropriate choice to run experiments on at lower fields (11.7 T and 7.05 T) where the sensitivity is not as good. Sample 9 was also considered interesting because of the slightly higher viscosity it exhibits.

The results of the T_1 and T_S measurements on **I** for liquid CO_2 at 7.05 T, 11.7 T and 16.4 T are presented in Table 22, along with the values first introduced in Table 5 for the deuterated common solvents for comparison.

Field (T)	**7.05**		**11.7**		**16.4**	
	T_1 (s)	T_S (s)	T_1 (s)	T_S (s)	T_1 (s)	T_S (s)
CO_2 (#8)	$\mathbf{63 \pm 3}$	$\mathbf{2458 \pm 317}$	$\mathbf{31.5 \pm 0.9}$	$\mathbf{1100 \pm 82}$	$\mathbf{17.6 \pm 0.1}$	$\mathbf{513 \pm 15}$
CO_2 (#9)	$\mathbf{51.9 \pm 0.8}$	$\mathbf{2354 \pm 141}$	$\mathbf{23 \pm 1}$	$\mathbf{778 \pm 46}$	$\mathbf{12.9 \pm 0.3}$	$\mathbf{297 \pm 19}$
Acetone	26 ± 2	1959 ± 163	12.6 ± 0.4	485 ± 16	6.9 ± 0.2	149 ± 5
Methanol	16.9 ± 0.6	1278 ± 87	7.69 ± 0.06	249 ± 9	4.17 ± 0.03	92.0 ± 0.9
Chloroform	15.4 ± 0.6	819 ± 34	6.53 ± 0.06	217 ± 3	3.55 ± 0.02	73 ± 1
Ethanol	10.3 ± 0.4	673 ± 27	4.51 ± 0.05	174 ± 2	2.46 ± 0.02	59.0 ± 0.6
DMSO	4.5 ± 0.2	468 ± 41	2.37 ± 0.02	194 ± 8	1.26 ± 0.01	73 ± 1
t-Butanol	2.2 ± 0.1	141 ± 6	1.18 ± 0.05	35 ± 1	0.684 ± 0.003	13.7 ± 0.3

Table 22: T_1 and T_S measurements of **I** with corresponding fitting errors for each of the different solvent environments (CO_2, acetone, methanol, chloroform, ethanol, DMSO and t-butanol) in order of increasing viscosity across three fields (7.05 T, 11.7 T and 16.4 T).

The values of T_1 and T_S measured are plotted against the inverse of the viscosity for all magnetic fields at which measurements were performed, in Figure 23. The viscosity value used for CO_2 is 0.08 mPa*s for Sample 8 and 0.15 mPa*s for Sample 9, as calculated in Table 19. For all of the plots the viscosity values for the deuterated solvents have been used as found in literature, with the exception of t-Butanol as the deuterated value could not be obtained, and therefore we use the protonated equivalent. The fits presented include only the common organic solvents and they extend to the expected value of CO_2.

In Figure 23, the solvents are abbreviated, in order to keep the graph legible. In order of increasing viscosity, they are as follows: **CO_2 (I)** corresponds to a viscosity of 0.08 mPa*s (Sample 8) and **CO_2 (II)** corresponds to a viscosity of 0.15 mPa*s (Sample 9), **A**. Acetone, **M**. Methanol, **Cl**. Chloroform, **E**. Ethanol, **D**. DMSO and **B**. t-Butanol.

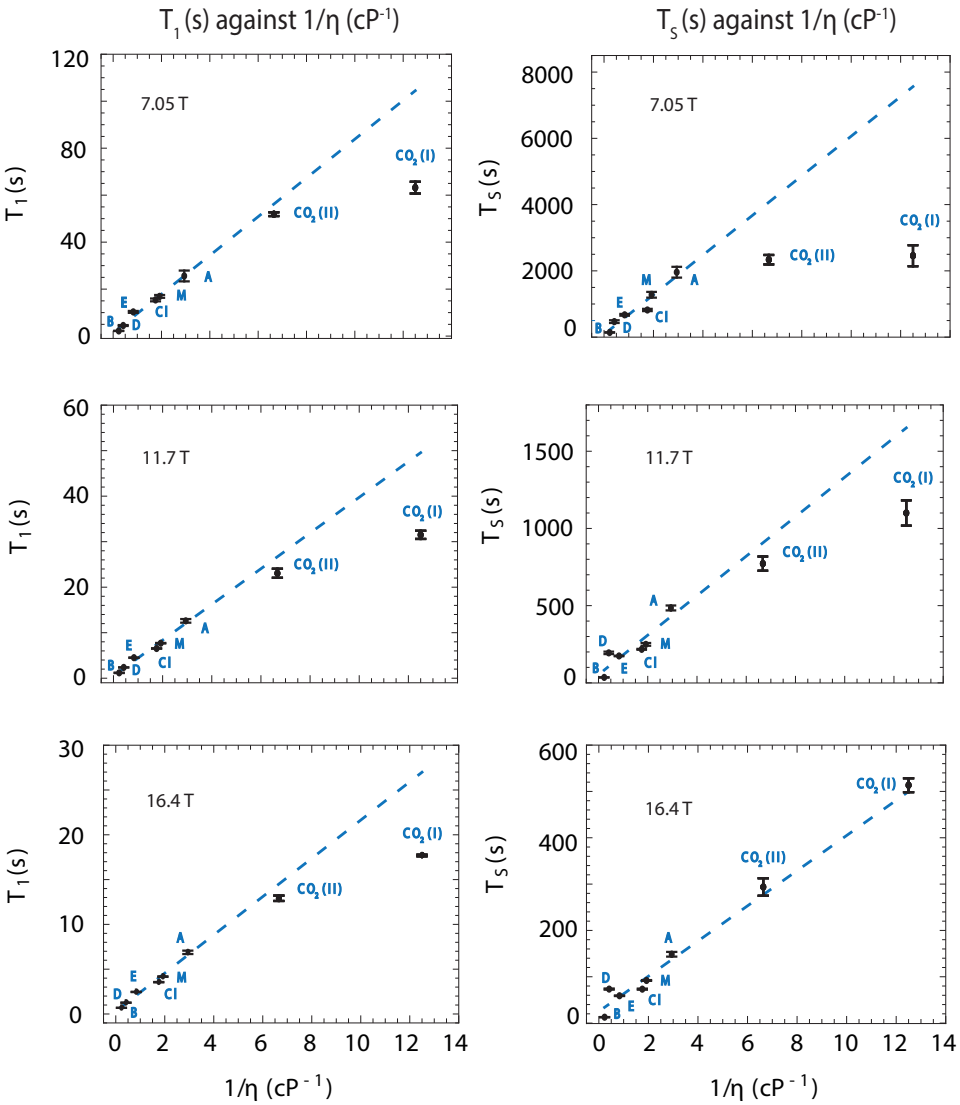

Figure 23: T_1 and T_S values of **I** plotted against the inverse of the viscosity $1/\eta$ of the dissolving medium (**CO_2 (I)** with η=0.08 mPa*s, **CO_2 (II)** with η=0.15 mPa*s, **A**. Acetone, **M**. Methanol, **Cl**. Chloroform, **E**. Ethanol, **D**. DMSO and **B**. t-Butanol) at three magnetic fields (7.05 T, 11.7 T and 16.4 T). The fit involves only the common organic solvents and it extends to the expected value of CO_2.

7.2.1 Discussion

The experimental data presented in Figure 23 suggest the following:

- For the T_1 measurements
  - In Sample 9 (**CO_2 (II)**) the viscosity of CO_2 is η=0.15 mPa*s. It appears that at this value the relaxation of **I** is similar to that in an organic solvent, resulting in good agreement with the trend established.

- In Sample 8 (**CO_2 (I)**) the viscosity of CO_2 is η=0.08 mPa*s. As such, it is closer to that of pure CO_2 than to an organic solvent. This reduced viscosity value results to deviation from the curve across all three fields (7.05 T, 11.7 T and 16.4 T).

- For the T_S measurements

  - The T_S values of **I** in CO_2 (**CO_2 (I) and CO_2 (II)**) at 16.4 T are in good agreement with the prediction made based on the common solvents. However, there appears to be a field dependence. As the field value decreases, the T_S value deviates further. We believe that the relevant relaxation mechanism taking effect is the Chemical Shift Anisotropy, as this relaxation mechanism is field dependent. It is also predicted to depend linearly to the inverse of the viscosity which is what is observed here.

Figure 24 aims to put this into context by comparing the different values across the three fields under discussion for Sample 8. Starting from the measured values of T_1 and T_S at 16.4 T, we calculated and plotted the theoretically expected values below, along with the actual ones. In the case the Chemical Shift Anisotropy is the relevant relaxation mechanism, then the singlet order values will be proportional to the square of the magnetic field.

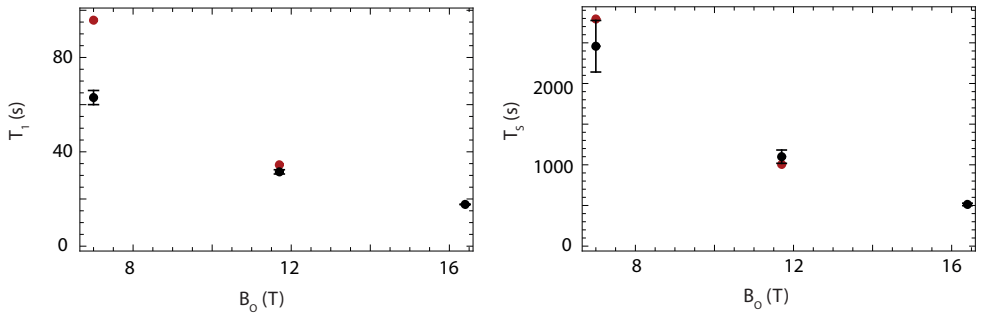

Figure 24: T_1 and T_S values of **I** in CO_2 (Sample 8) plotted against the magnetic field. The black series demonstrates experimental points acquired across the three fields (7.05 T, 11.7 T and 16.4 T), and the corresponding fitting error as derived from Mathematica. The red series consists of calculated values starting from the experimental values acquired at 16.4 T and assuming that they scale with the square of the magnetic field.

For T_1 at higher fields the CSA dominates as there is a good agreement between the experimental (black) and the predicted (red) values. At 7.05 T the CSA becomes less important and the relaxation is dominated by DD as one would expect, and therefore deviates from the curve. For T_S it appears that CSA holds well even at lower fields as the singlet is immune to DD relaxation. However, at 7.05 T despite the values being within error, the experimental point is lower. This is suggesting that a different relaxation mechanism, possibly spin rotation, is becoming dominant. Figure 24 confirms the hypothesis as the T_S values scale with the square of the magnetic field.

7.2.2 Conclusions

There appears to be an upper limit to how much the lifetimes T_1 and T_S can be extended with decreasing viscosity. In the case of T_S it seems that the Chemical Shift Anisotropy is the dominant mechanism, and prevents the observation of the theoretically expected maximum.

Despite the deviation from the expected value, we have achieved a T_S of around 40 minutes at high field (7.05 T). To put this into context, the longest recorded singlet lifetime to this date is 66 minutes. This has been achieved during a previous study [8] using the same molecule, **I**, measured in acetone at very low field (0.002T).

We therefore expect a T_S value of **I** in CO_2 to be even greater at low magnetic field, exceeding the 66 minute record.

7.3 Temperature Study

7.3.1 Motivation

So far the results presented give the impression that measurements of T_1 and T_S values are not possible in the supercritical regime. That is not true, and for that reason we present in this section a series of experiments that aim to prove that. This section discusses T_1 and T_S experiments conducted on **I** in liquid and supercritical CO_2 conducted at 11.7 T and 16.4 T according to Table 1. The sample used was Sample 9, details of which can be found in Table 14.

7.3.2 Observations

Figure 25 presents a multiple display of ^{13}C spectra of **I** in CO_2 (Sample 9) acquired at 11.7 T according to Table 1 for a range of temperatures (23 °C - 43 °C). The results are presented in Table 23. It is interesting that unlike Sample 3, which was presented in Figure 15, the Naphthalene signal does not disappear. T_1 as well as T_S values can be measured up to 43 °C. The CO_2 peak loses intensity significantly at 39 °C, which might be an indication as to where the transition point is. We attribute this difference between the behaviour of Samples 3 and 9 to the presence of the insert within the tube.

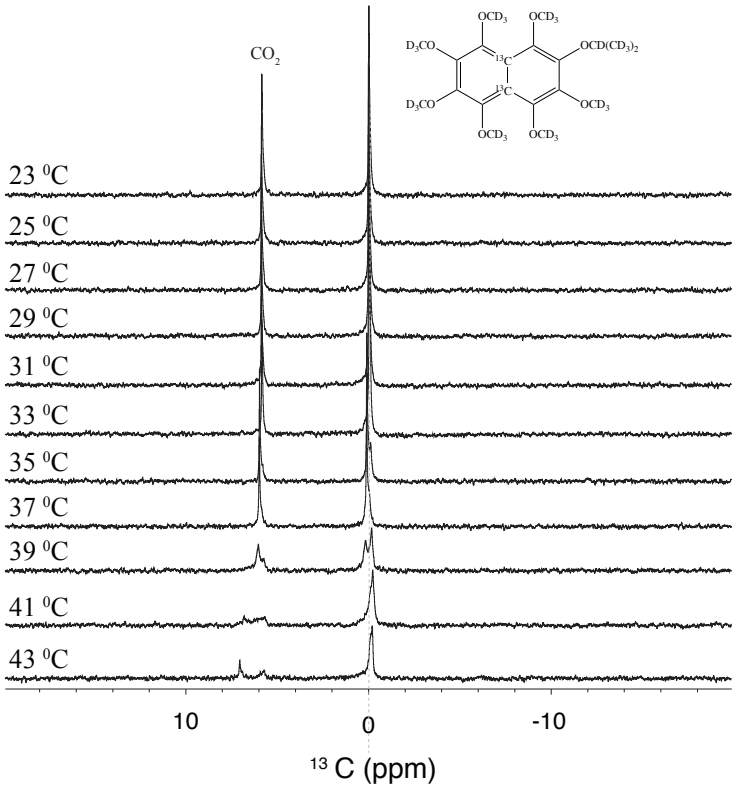

Figure 25: Multiple display of ^{13}C spectra of Sample 9 (**I** in CO_2) acquired at 11.7 T at a temperature range from 23 °C to 43 °C. The results are given in Table 23. The peak centered at 0 ppm is belongs to **I** and the one on the left belongs to CO_2. All spectra are acquired with the heater on. The transmitter is on resonance with the peak of **I**, and has been referenced as point 0 in the ppm scale.

Figure 26 depicts a multiple display of ^{13}C spectra of **I** in CO_2 (Sample 9) acquired at 16.4 T according to Table 1 for a range of temperatures (22 °C - 40 °C). The peak around 125 ppm belongs to CO_2 while the one around 118 ppm belongs to **I**.

The behaviour of Sample 9 at two different fields (11.7 and 16.4 T) with the increase of temperature is consistent. T_1 and T_S measurements were possible up to 40 °C and the results are presented in Table 23.

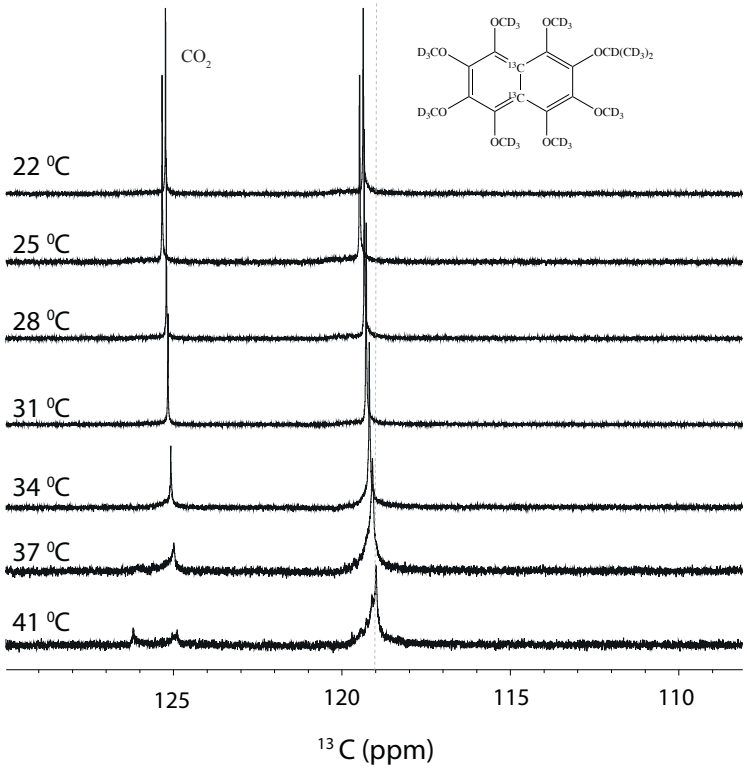

Figure 26: Multiple display of ^{13}C spectra of Sample 9 (**I** in CO_2) acquired at 16.4 T while varying the temperature from 22 °C to 40 °C. The peak around 120 ppm belongs to **I** and the one around 135 ppm belongs to CO_2. All spectra are acquired with the heater on. This figure is referenced against TMS.

7.3.3 Discussion

The results of the measurements on T_1 and T_S on ^{13}C for **I** in CO_2 conducted at 11.7 T and 16.4 T are presented in Table 23. For both magnetic fields the longest T_1 and T_S appear for different temperatures. At 11.7 T, those are 37 °C and 35 °C for T_1 and T_S respectively. At 16.4 T they are 25 °C and 28 °C respectively.

The T_S decay curves fit a monoexponential decay profile well at all temperatures without exception, suggesting the hypothesis made earlier on the convection was correct. In

T (°C)	11.7 (T)		16.4 (T)	
	T_1 (s)	T_S (s)	T_1 (s)	T_S (s)
22			12.9 ± 0.3	297 ± 19
23	25 ± 1	827 ± 45		
25	25 ± 1	792 ± 38	13.1 ± 0.5	320 ± 24
27	24 ± 1	876 ± 46		
28			12.6 ± 0.2	324 ± 27
29	23 ± 1	781 ± 51		
31	25 ± 1	773 ± 43	12.3 ± 0.3	309 ± 24
33	20.2 ± 0.9	833 ± 56		
34			11.4 ± 0.2	283 ± 21
35	21 ± 2	930 ± 48		
37	26 ± 2	833 ± 81	10.7 ± 0.2	264 ± 18
39	23 ± 2	787 ± 68		
40			8.8 ± 0.2	227 ± 17
41	19 ± 3	701 ± 51		
43	16 ± 2	602 ± 56		

Table 23: T_1 and T_S values of **I** in CO_2 (Sample 9) acquired at 11.7 T and 16.4 T according to Table 1 over a range of temperatures spanning from 22 °C to 43 °C.

Figure 27 the fits of the singlet order decay for the highest temperature at each field are presented. Those correspond to 40 °C at 16.4 T and 43 °C at 11.7 T. At the higher field the curve has 16 points while at the lower field the curve has only 10 points. As the relaxation is much slower at 11.7 than at 16.4 T, this serves to shorten the experimental times.

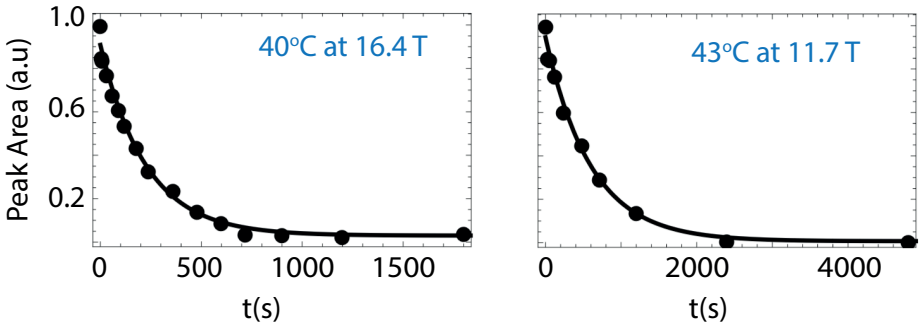

Figure 27: Singlet order decay curve fits as a function of time at the maximum temperatures where measurements were conducted: 40 °C at 16.4 T and 43 °C at 11.7 T for Sample 9 of **I** in CO_2. The decay is monoexponential and the fits are satisfactory even at high temperatures. At 16.4 T the fit consists of 16 points while at 11.7 T the curve has only 10 points. The reason for this is to shorten the experimental time as the decay is much slower at the lower field.

Figure 28 presents the T_1 and T_S values of **I** in CO_2 (Sample 9) as measured at 11.7 T and 16.4 T against the temperature. At 11.7 T the data are more dispersed but the general trend that can be observed in all cases is a decrease of T_1 and T_S values as the temperature increases.

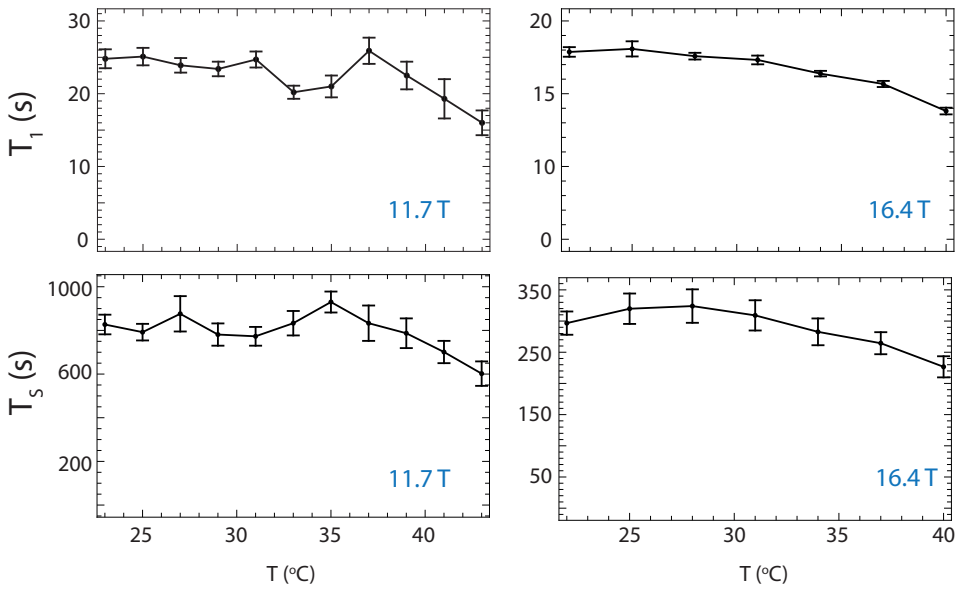

Figure 28: T_1 and T_S of **I** in CO_2 (Sample 9) plotted against temperature at 11.7 T and 16.4 T. Data were acquired according to Table 1. Sample 9 was prepared according to Table 14.

7.3.4 Conclusions

The most important conclusion from this study is that measurements of T_1 and T_S at supercritical CO_2 are possible. We attribute the loss of signal of **I** mentioned at Section 7.6, where the preliminary experiments on **I** in CO_2 are presented, to the very fast motion of I outside the coil region and the consequent loss of the signal. The use of inserts appears to remedy that.

The monoexponential decay curves of the singlet order produced, present a good indication that convection does not pose an insurmountable obstacle in the measurements in CO_2 at elevated temperatures.

An overall decreasing trend is observed with increase of temperature at both fields for both T_1 and T_S values. This would merit from further investigation to identify whether a relaxation mechanism like SR is becoming dominant in the supercritical regime, leading to this phenomenon.

7.4 T_1 and T_S Measurements of Substituted Acetylene in CO_2

The measurements on **III** in the common organic solvents under discussion (acetone, methanol, chloroform, ethanol, DMSO and t-butanol) conducted at 16.4 T were complemented by a measurement in CO_2. The details of the sample preparation are mentioned in Table 15. The results are presented in Table 24, along with the previous results from Table 8. The viscosity of CO_2 is calculated as discussed in Section 8.1.3, but the rest of the values used are from literature.

Solvent	**Viscosity (mPa*s)**	T_1 **(s)**	T_S **(s)**	**D *10^{-9} (m^2/s)**
CO_2	0.09	18.2 ± 0.2	211 ± 3	10.8 ± 0.05
Acetone	0.34	8.2 ± 0.1	249 ± 11	3.2 ± 0.02
Methanol	0.52	6.40 ± 0.06	207 ± 11	2.0 ± 0.009
Chloroform	0.57	4.50 ± 0.07	206 ± 4	1.8 ± 0.02
Ethanol	1.2	4.43 ± 0.06	159 ± 7	1.3 ± 0.03
DMSO	2.4	2.07 ± 0.02	-	0.58 ± 0.003
t-Butanol	4.3	1.52 ± 0.02	23.7 ± 0.5	0.42 ± 0.003

Table 24: T_1, T_S and diffusion coefficient measurements of **III** with corresponding fitting errors for each of the different solvent environments (CO_2, acetone, methanol, chloroform, ethanol, DMSO and t-butanol) in order of increasing viscosity at 16.4 T. Data acquired according to Table 1. The samples were made according to Table 4 and Table 15 The viscosity values reported are the ones found in literature.

7.4.1 Discussion

The values of T_1 and T_S measured are plotted against the inverse of viscosity at 16.4 T in Figure 29. For all of the plots the viscosity values for the deuterated solvents have been used, with the exception of t-butanol, and the value of the viscosity of CO_2 has been calculated from the diffusion coefficient of **III** in CO_2 and in methanol as first presented in Section 7.1.3.

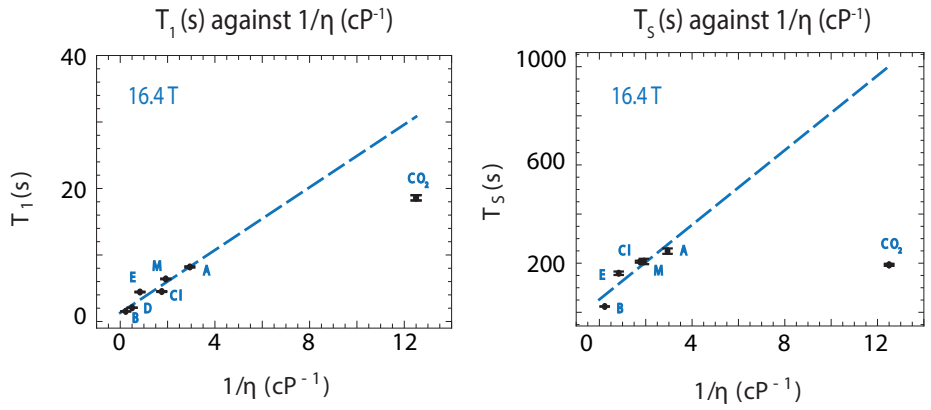

Figure 29: T_1 and T_S plots against the inverse of the viscosity at 16.4 T for **III** in different solvent environments: $\mathbf{CO_2}$ with a calculated η=0.09 mPa*s, **A**. Acetone, **M**. Methanol, **Cl**. Chloroform, **E**. Ethanol, **D**. DMSO and **B**. t-Butanol. The fit involves only the common organic solvents and it extends to the expected value of CO_2. The T_S plot does not include a point for DMSO as the conditions for the transfer of magnetization to singlet could not be identified.

The T_1 and T_S values of **III** in CO_2 deviate from the trend set by the organic solvents. In the case of the T_S, the value is lower than that measured in acetone: 211s and 249s respectively. It is interesting how the T_S values of **III** in both CO_2 and t-butanol deviate from the curve. As can be seen in Figure 30, in both of those solvent environment, the expected ^{13}C peak of **III** is also split into a doublet.

The reasons for this are unclear at this point and may merit from further investigation, it could however be that the molecule **III** is assuming a different spatial conformation in those solvents. This could possibly change the chemical shift difference value between the spin pair, allowing for the J-coupling to be visible on the spectrum in the form of a splitting between the two peaks. The fact that the M2S sequence works, eliminates the possibility that we have moved away from the near-equivalence regime, however, it could be that different spatial conformation causes the relaxation to occur faster.

As mentioned earlier, the reason why the series of experiments on **III** were conducted, was because it has been found in the past to be resistant to the Chemical Shift Anisotropy relaxation mechanism. Despite the not very encouraging results so far, we decided to measure Sample 10 at 7.05 T in order to see if the T_1 and T_S values change with field. The results are given in Table 25. The T_1 and T_S values are not independent of the field as we would expect in the case that Chemical Shift Anisotropy was not a relevant relaxation mechanism.

Field (T)	T_1 **(s)**	T_S **(s)**
16.4	18.2 ± 0.2	211 ± 3
7.05	70 ± 4	861 ± 137

Table 25: T_1 and T_S measurements of **III** in CO_2 (Sample 10) with corresponding fitting errors at 16.4 T and 7.06 T. Data acquired according to Table 1. The sample was made according to Table 15.

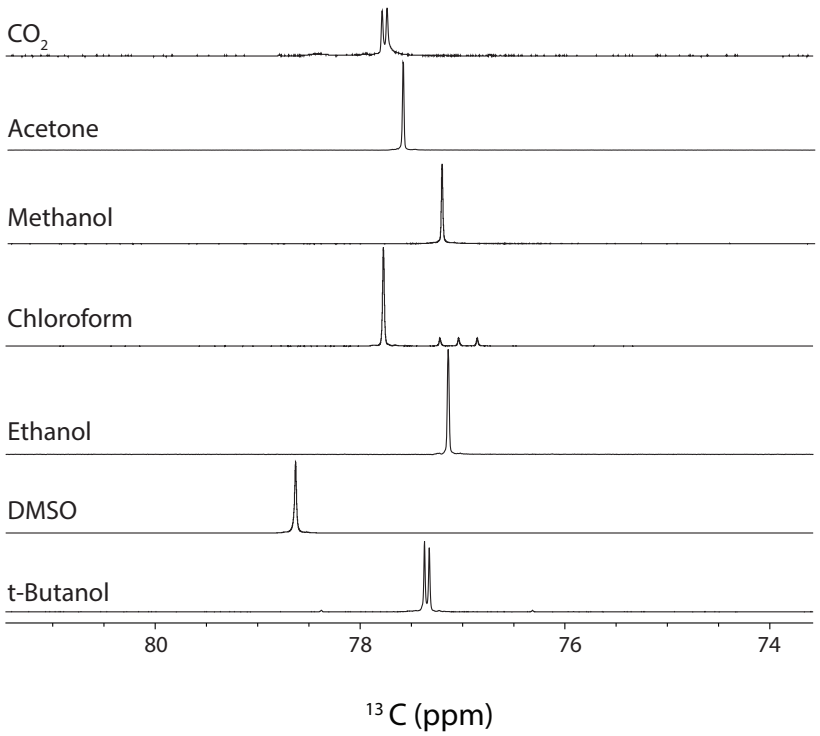

Figure 30: Multiple display of ^{13}C spectra of **III** for each of the different solvent environments (CO_2, acetone, methanol, chloroform, ethanol, DMSO and t-butanol) in order of increasing viscosity at 16.4 T. The triplet belonging to chloroform can also be seen in the chloroform ^{13}C spectrum. The samples was prepared according to Tables 4 and 15.

7.4.2 Conclusions

Unfortunately, it seems that **III** is not as resistant to Chemical Shift Anisotropy as hypothesized originally. The values of **III** in t-butanol and CO_2 deviate from the expected and for **III** in DMSO, the measurement of T_S was impossible. **III** is not an ideal system to work with. A different molecule needs to be selected for future experiments.

8 Summary

A series of experiments which verified the prediction about a linear trend between the inverse of the viscosity $1/\eta$ and T_1 was conducted. A second series of experiments proved that a similar trend holds for the T_S, for which no predictions had been made.

By extending the study to solvents of extremely low viscosity, in particular liquid and supercritical CO_2, we discovered that measurements in the supercritical regime have proven to be complex, but not impossible. However, we found the liquid regime easier to work with in this preliminary stage of this investigation.

We did not encounter any solubility issues with the compounds used in liquid CO_2, which is encouraging. However, convection manifesting through a two component decay, poses a real hindrance to the measurements in CO_2, leading to reduced observed T_S. Since spinning is not an option in the case of a high pressure sample, restriction of the sample within the active area of the detection coil was tried with an insert. After numerous attempts, we now have a design that gives meaningful data.

Both T_1 and T_S values increase significantly while going from an organic solvent to liquid CO_2. For viscosities of liquid CO_2 close to those of organic solvents, we recover the theoretical maximum.

With lowering viscosity to values that are closer to that of pure CO_2, have observed a deviation from the theoretical maximum. Therefore, there appears to be an upper limit to how much the lifetimes T_1 and T_S can be extended with decreasing viscosity. In the case of T_S it seems that the Chemical Shift Anisotropy is the dominant mechanism, and prevents the observation of the theoretically expected maximum.

We have determined a range of concentrations for the main system under investigation (**I** in CO_2) where both the viscosity and the T_S remain practically invariant while allowing for a better signal to noise ratio and thus enabling measurements in a range of magnetic fields.

By optimizing the insert design, concentration and preparation, we have achieved a T_S of around 40 minutes (**I** in liquid CO_2) at high field (7.05 T). The longest recorded singlet lifetime to this date is 66 minutes (**I** in acetone) at very low field (0.002T).[8]

We therefore expect a T_S value of **I** in CO_2 to be even greater at low magnetic field, exceeding the 66 minute record.

In trying a different system (**III** in CO_2), which was believed to be resistant to the Chemical Shift Anisotropy relaxation mechanism, we concluded in that the system was not ideal for the purpose of this investigation and therefore a different one needs to be selected in order to progress.

9 Future Work

The ultimate goal of this project is to combine hyperpolarization with long lived states, so steps will be taken towards that direction.

The rate of relaxation of singlet order decreases with decreasing field. Even lower fields will be explored with CO_2 as the solvent in order to achieve longer lifetimes.

Measurements of pressure, temperature and viscosity will be done in order to build accurate phase diagrams of our systems. For this, Dr. F. Giustiniano is already building equipment.

Future experiments will focus on broadening our understanding of the behaviour of **I** in CO_2 by exploring how different CO_2 densities and/or different mixtures influence the critical point, T_1 and T_S. Different ways of approaching the theoretical values will be explored and if that is not possible and explanation will be sought for the phenomena which cause the CO_2 to exhibit lower than the expected values.

As has been made obvious, the results of each experiment are highly dependent one the conditions of the sample (volume, concentration, pressure). The ideal conditions to work with for each new system will be sought.

There is an indication that in the supercritical regime a different relaxation mechanism becomes prominent (possibly spin rotation) and merits further investigation.

Other molecular systems will need to be investigated in order to understand the role of different relaxation mechanisms under low viscosity conditions.

References

[1] D. R. Lide, editor. *CRC Handbook of Chemistry and Physics*. CRC Press, 74th edition, 1993 - 1994.

[2] M. Carravetta and M. H. Levitt. Theory of long-lived nuclear spin states in solution nuclear magnetic resonance. I. Singlet states in low magnetic field. *J. Chem. Phys.*, 122(21):214505, 2005.

[3] A. Fenghour, W. A. Wakeham, and V. Vesovic. The Viscosity of Carbon Dioxide. *J. Phys. Chem. Ref. Data*, 27(1):31–44, 1998.

[4] J. H. Ardenkjær-Larsen, B. Fridlund, A. Gram, G. Hansson, L. Hansson, M. H. Lerche, R. Servin, M. Thaning, and K. Golman. Increase in signal-to-noise ratio of $>$ 10,000 times in liquid-state NMR. *Proc. Natl. Acad. Sci. USA*, 100(18):10158 – 10163, 2003.

[5] S. G. J. van Meerten, M. C. D. Tayler, A. P. M. Kentgens, and P. J. M. van Bentum. Towards Overhauser DNP in supercritical CO_2. *J. Magn. Reson.*, 267:30–36, 2016.

[6] M. H. Levitt. *Spin Dynamics, Basics of Nuclear Magnetic Resonance*. Wiley, 2nd edition, 2008.

[7] T. D. W. Claridge. *High-Resolution NMR Techniques in Organic Chemistry*. Elsevier, 2nd edition, 2009.

[8] G. Stevanato, J. T. Hill-Cousins, P.r Håkansson, S. S. Roy, L. J. Brown, R. C. D. Brown, G. Pileio, and M.H. Levitt. A Nuclear Singlet Lifetime of More than One Hour in Room-Temperature Solution. *Angew. Chem. Int. Ed.*, 54(12):3740–3743, 2015.

[9] J. Kowalewski and L. Maler. *Nuclear Spin Relaxation in Liquids: Theory, Experiments, and Applications*. Taylor & Francis, 1st edition, 2006.

[10] G. Pileio, J. T. Hill-Cousins, S. Mitchell, I. Kuprov, L. J. Brown, R. C. D. Brown, and M. H. Levitt. Long-Lived Nuclear Singlet Order in Near-Equivalent 13C Spin Pairs. *J. Am. Chem. Soc.*, 134(42):17494–17497, 2012.

[11] M. Carravetta and M. H. Levitt. Long-Lived Nuclear Spin States in High-Field Solution NMR. *J. Am. Chem. Soc.*, 126(20):6228–6229, 2004.

[12] G. Pileio, M. Carravetta, E. Hughes, and M. H. Levitt. The Long-Lived Nuclear Singlet State of 15N-Nitrous Oxide in Solution. *J. Am. Chem. Soc.*, 130(38):12582–12583, 2008.

[13] G. Stevanato, S. S. Roy, J. Hill-Cousins, I. Kuprov, L. J. Brown, R. C. D. Brown, G. Pileio, and M. H. Levitt. Long-lived nuclear spin states far from magnetic equivalence. *Phys. Chem. Chem. Phys.*, 17:5913–5922, 2015.

[14] M. C. D. Tayler and M. H. Levitt. Singlet nuclear magnetic resonance of nearly-equivalent spins. *Phys. Chem. Chem. Phys.*, 13:5556–5560, 2011.

[15] G. Pileio. Relaxation theory of nuclear singlet states in two spin-1/2 systems. *Prog. Nucl. Magn. Reson. Spectrosc.*, 56(3):217 – 231, 2010.

[16] G.Pileio and M. H. Levitt. Theory of long-lived nuclear spin states in solution nuclear magnetic resonance. II. Singlet spin locking. *J. Chem. Phys.*, 130(21): 214501, 2009.

[17] M. Carravetta, O. G. Johannessen, and M. H. Levitt. Beyond the T_1 Limit: Singlet Nuclear Spin States in Low Magnetic Fields. *Phys. Rev. Lett.*, 92:153003, 2004.

[18] G. Brunner. Supercritical fluids: technology and application to food processing. *J. Food. Eng.*, 67(1):21–33, 2005.

[19] Langley G.J. Supercritical Fluid Chromatography (SFC), July 2018. URL `https://www.southampton.ac.uk/ gjl/Research/sfc.htm`.

[20] E. Klesper, A. H. Corwin, and D. A. Turner. High Pressure Gas Chromatography above Critical Temperature. *J. Org. Chem.*, 27(2):700–701, 1962.

[21] F. Li and Y. Hsieh. Supercritical fluid chromatography-mass spectrometry for chemical analysis. *J. Sep. Science*, 31(11-12):1231–1237, 2008.

[22] W. P. Farrell, C. M. Aurigemma, and D. F. Masters-Moore. Advances in High Throughput Supercritical Fluid Chromatography. *J. Liq. Chromatogr. Relat. Technol.*, 32(11-12):1689–1710, 2009.

[23] D. Sykora, J. Vozka, and E. Tesarova. Chromatographic methods enabling the characterization of stationary phases and retention prediction in high-performance liquid chromatography and supercritical fluid chromatography. *J. Sep. Science*, 39 (1):115–131, 2015.

[24] A. Tarafder. Metamorphosis of supercritical fluid chromatography to SFC: An Overview . *Tr. Anal. Chem.*, 81(1):3–10, 2016.

[25] United States Environmental Protection Agency. Overview of Greenhouse Gases, Carbon Dioxide Emissions, August 2018. URL `https://www.epa.gov/ghgemissions/overview-greenhouse-gases`.

[26] D. Speybrouck and E. Lipka. Preparative supercritical fluid chromatography: A powerful tool for chiral separations. *J. Chromatogr. A*, 1467:33–55, 2016.

[27] P. Raveendran, Y. Ikushima, and S. L. Wallen. Polar Attributes of Supercritical Carbon Dioxide . *Acc. Chem. Res.*, 38(6):478–485, 2005.

[28] K. Albert. Supercritical fluid chromatography-proton nuclear magnetic resonance spectroscopy coupling . *J. Chromatogr. A*, 785(1):65–83, 1997.

[29] G. Pileio, M. Carravetta, and M. H. Levitt. Storage of nuclear magnetization as long-lived singlet order in low magnetic field. *Proc. Natl. Acad. Sci. USA*, 107(40): 17135–9, 2010.

[30] A. Jerschow and N. Müller. 3D Diffusion-Ordered TOCSY for Slowly Diffusing Molecules. *J. Magn. Reson. Series A*, 123(2):222–225, 1996.

[31] A. Jerschow and N. Müller. Suppression of Convection Artifacts in Stimulated-Echo Diffusion Experiments. Double-Stimulated-Echo Experiments. *J. Magn. Reson.*, 125(2):372–375, 1997.

[32] J. T. Hill-Cousins, I.-A. Pop, G. Pileio, G. Stevanato, P. Håkansson, S. S. Roy, M. H. Levitt, L. J. Brown, and R. C. D. Brown. Synthesis of an Isotopically Labeled Naphthalene Derivative That Supports a Long-Lived Nuclear Singlet State. *Org. Lett.*, 17(9):2150–2153, 2015.

[33] G. Pileio, S. Bowen, C. Laustsen, M. C. D. Tayler, J. T. Hill-Cousins, L. J. Brown, R. C. D. Brown, J. H. Ardenkjaer-Larsen, and M. H. Levitt. Recycling and Imaging of Nuclear Singlet Hyperpolarization. *J. Am. Chem. Soc.*, 135(13):5084–5088, 2013.